DIPLOMARBEIT

Durability of Catalytic Coatings on Hollow Micro Glass Spheres used in a Hybrid Hydrogen Storage System

Ausgeführt am Institut für
Festkörperphysik
der Technischen Universität Wien

Betreuer:

Ao.Univ.Prof. Dipl.-Ing. Dr.techn. Christoph EISENMENGER-SITTNER

von

Clara Oppolzer

Albertgasse 33/2, 1080 Wien

Juni 2019

Declaration

I hereby declare and confirm that this thesis is entirely the result of my own original work. Where other sources of information have been used, they have been indicated as such and properly acknowledged. I further declare that this or similar work has not been submitted for credit elsewhere.

Vienna, June 10, 2019

Clara Oppolzer

Acknowledgement

First, I would like to thank Prof. Christoph Eisenmenger-Sittner for his continuous, thoughtful supervision and kind support. Also, I would like to express my special thanks of gratitude to Dipl.Ing. David Boehm for his immense helpfulness. I am very grateful for the caring support experienced from the team and for this given chance to apply and broaden my recent knowledge.

Kurzfassung

In dieser Diplomarbeit wird eine hybride Wasserstoff Speicher Lösung diskutiert, die physische Speicherung in hohlen Glas Mikrokugeln und chemische Speicherung in Natrium Borhydrid kombiniert. Die hohlen Glas Mikrokugeln können nur bei erhöhten Temperaturen beladen und entladen werden. Die chemische Reaktion zwischen Wasser und Natrium Borhydrid, die den Wasserstoff vom Natrium Borhydrid trennt, produziert Hitze. So wird also die Hitze, die durch die Reaktion entsteht verwendet, um den Wasserstoff aus den hohlen Glas Mikrokugeln zu entladen. Die Reaktion von Natrium Borhydrid und Wasser benötigt einen Katalysator, der auf die hohlen Glas Mikrokugeln aufgebracht wird. Da die Katalysatorschicht bei jeder Reaktion abgenutzt wird, sind zur Zeit vier Wasserstoff Zyklen möglich, bis der Katalysator komplett abgetragen ist. Vier Wasserstoff Zyklen bedeutet, dass die selben Mikroglas Kugeln vier Mal beladen und wieder entladen werden können. Aus ökonomischen und ökologischen Gründen wird es angestrebt, die selben Glas Mikrokugeln so oft wie möglich zu verwenden. Innerhalb dieser Diplomarbeit wurden Untersuchungen zur Stabilität des Katalysators gemacht. Dazu wurden ungeladene Glas Mikrokugeln verwendet, um den Fokus auf die Reaktion und damit den Katalysator zu legen. Nichtsdestotrotz wurden theoretische Berechnungen gemacht die zeigen, wieviel Wasserstoff bei den Reaktionen die Glas Mikrokugeln verlassen würde.

Abstract

Within this thesis a hybrid hydrogen storage solution is discussed that combines physical storage in hollow glass micro spheres and chemical storage in sodium borohydride. The hollow glass micro spheres can only be loaded and unloaded at elevated temperatures. The chemical reaction between water and sodium borohydride that separates the hydrogen from the sodium borohydride, produces heat. Thus, the heat that arises due to the reaction, is used to unload the hydrogen from the hollow glass micro spheres. The reaction of sodium borohydride with water requires a catalyst that is coated onto the hollow glass micro spheres. As the catalyst wears off at each reaction, only four hydrogen cycles are currently possible with the same set of coated hollow glass micro spheres, until the catalyser is completely removed. Four hydrogen cycles means that the same glass micro spheres can be loaded and unloaded four times. For economical and ecological reasons, the hollow glass micro spheres are sought to be used as many times as possible. Hence, within this thesis, investigations into the stability of the catalyser layer were performed. For this purpose, all experiments were conducted with unloaded micro spheres, to put the focus on the reaction and therefore the catalyser. Nonetheless, theoretical calculations were made that show how much hydrogen would leave the glass micro spheres during the reactions.

Contents

1 Introduction

One of the main issues human society is facing is environmental pollution, fossil fuels being the principle source. Fossil fuels such as coal and gasoline have been maintained as the key source of energy, as they provide cheap and efficient ways to generate electricity or mechanical work. Their widespread use has led to environmental hazards related to both their finite reserves (oil and gas: 40 more years, coal: 50-100 years) and consequent release of pollutant gases and waste materials [1]. Therefore, there is an ever growing concern to produce and provide alternative, cleaner sources of energy. There are existent solutions which are already used for large scale energy production, like nuclear energy. However, the problem of safety and disposal raises its own set of concerns regarding environmental jeopardy [2]. Amongst the available renewable energy sources are wind generators, conventional solar panels, focused arrays, geothermal, wave and tidal generators which directly convert natural energy (like solar and wind energy) into electricity. The general problem associated with renewable sources is one of geographical location especially in the case of geothermal, wind and tide power [3]. These energy sources are not always located close to populated areas and thus suffer the inefficiency of long range transportation. Secondly, the storage of energy for supply based on demand has yet to be resolved, that is to say it is not always windy and it is not always sunny. However the demand of electricity is somewhat constant. A possible solution to the problems listed above is the use of the hydrogen cycle (figure 1.1), which would operate as a battery to

store renewable energy. Thus, there exists a firm interest in hydrogen based energy technologies, such as solar/wind driven production of hydrogen via electrolysis of water and its use within direct hydrogen combustion and within hydrogen fuel cells. Hydrogen is a secondary energy source and regarded as one of the best means to store primary energies such as wind and solar power [4] due to its abundant occurrence in the universe.

This work will focus solely on hydrogen storage, namely a hybrid concept, consisting of catalyst sputter-coated hollow glass micro spheres and sodium borohydride. The hollow spheres can be loaded with hydrogen by applying a pressure of 70 MPa. They are heated to 250 ° C to let the hydrogen diffuse through the glass into the micro spheres. When the system is cooled down to room temperature, the hydrogen is trapped inside the spheres. To release the hydrogen at combustion, heat is applied by an exothermic hydrolytic reaction, here: sodium borohydride and water. A crucial point of this storage technique is the re-usability of the hollow glass micro spheres, which is limited by the durability of a ruthenium catalyst coating on the spheres that is enhancing the reaction speed.

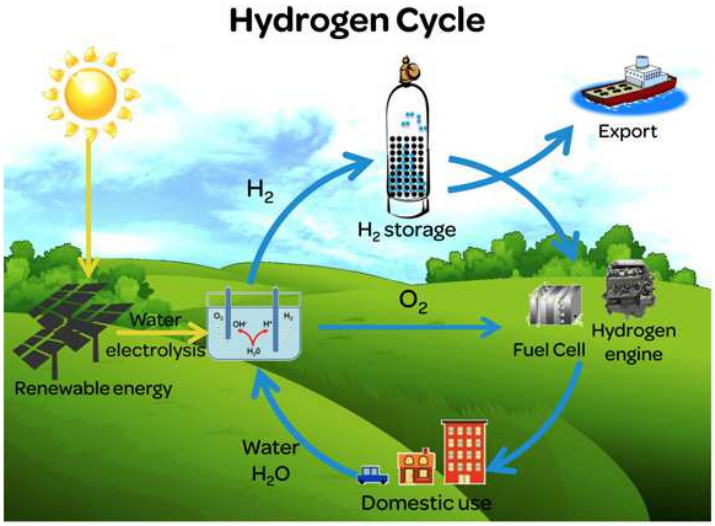

Figure 1.1: Hydrogen Cycle [5]

Hence, this work aims to prolong the usability of the hollow glass micro spheres, as previous investigators managed a total number of four cycles without a considerable decrease in hydrogen yield [6, 7]. More precisely, this work aims to investigate means to increase the adhesion of the catalyst layers as their depletion is the main reason why the spheres are not usable more than four times so far.

2 Theory & State of the Art

This chapter presents the relevant theory and fundamentals applied within this thesis, combined with the state of the art within the topics. Different hydrogen storage systems and the properties and different fabrication processes of HGMS will be discussed. At last the hybrid hydrogen storage system and the role of the catalyst within this system will be explained.

2.1 Hydrogen Storage

As hydrogen as an alternative energy carrier has the main disadvantage of its explosiveness that bears safety hazards, lots of research is done on its safe storage. These storage methods can be broadly classified into physical and chemical storage (figure 2.1). The most common chemical storage solutions are either absorption of hydrogen by hydrides, Liquid Organic Hydrogen Carriers (LOHC) or electrochemical storage of hydrogen that is adsorbed on metallic alloys (figure 2.1). Physical storage has four subcategories, namely: absorption on solid material as well as solid, liquid and gaseous storage.

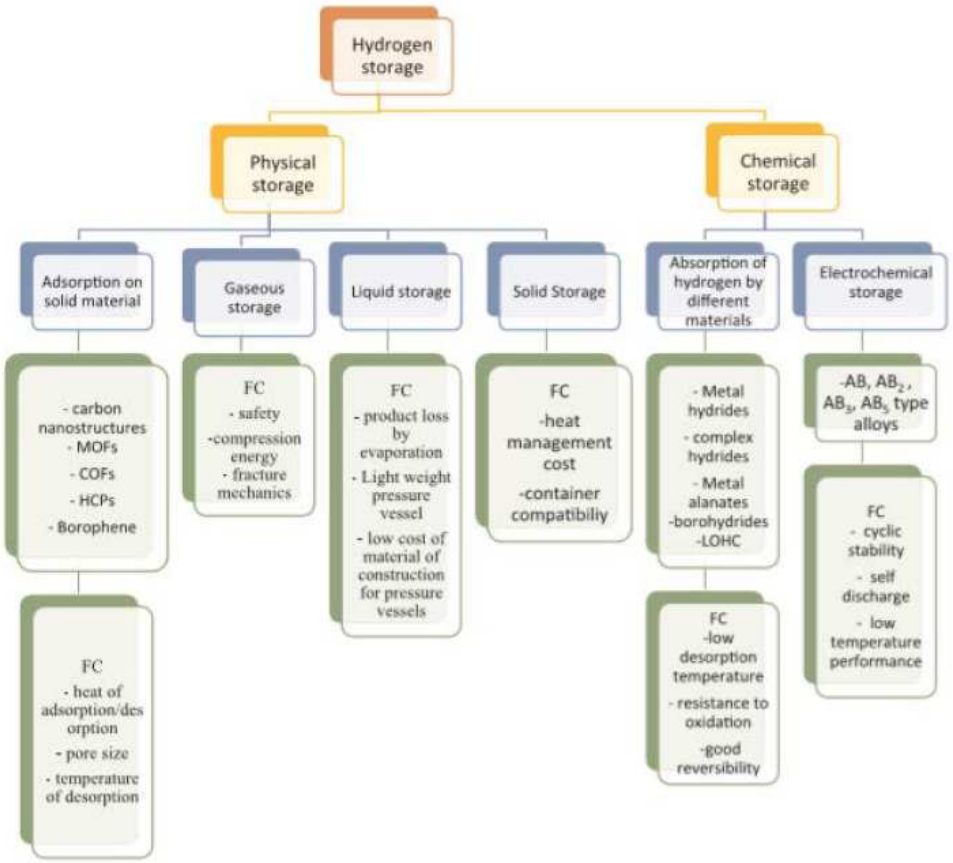

Figure 2.1: Different hydrogen storage methods together with their future challenges (FC) and possible materials. Taken from [8]

2.1.1 Chemical Storage

In chemical storage, hydrogen is covalently bonded on liquid or solid sate storage material. Primarily used materials are ammonia, metal hydrides such as sodium borohydride $NaBH_4$ [9, 10, 11, 12, 13, 14, 15, 16] formic acid or liquid organic hydrogen carriers (LOHC)[17]. Chemical storage includes absorption in a solid or liquid material and adsorption, hence electrochemical storage. Electrochemical storage [18, 19] releases the bonded hydrogen with electricity rather than heat (thermochemical storage).

Teichmann et. al. [17] founded the start-up Hydrogenious in 2013 and patented their hydrogen storage system that comprises hydrogen storage in liquid organic hydrogen carriers (LOHC), which found great medial resonance. They are currently demonstrating their technology in a project in Erlangen together with Fraunhofer Instiute, where hydrogen is produced with solar power and then used to power electric cars and launched another project in 2016 together with Siemens. As the LOHC can be stored in plastic tanks, the hydrogen transportation is profitable for distances of up to 600 km, instead of 200 km, according to Teichmann [20].

2.1.2 Physical Storage

In physical storage, hydrogen is either stored in its molecular form by adsorption on a solid material or in its gaseous, liquid or solid state [21, 22]. Materials to store it in its molecular form include carbon nano-tubes [23, 24, 25], graphene [26, 27], metal organic frameworks (MOFs)[28], covalent organic frameworks (COFs) and clathrate hydrates. Storing of hydrogen in its solid, liquid or gaseous form comprises challenges that makes intensive research necessary. Liquefied storage requires cryogenic temperatures and faces the problem of hydrogen loss due to vaporisation. Gaseous storage in pressure vessels make high pressures necessary, which gives rise to safety issues. These safety issues can be overcome by storing hydrogen in hollow glass micro spheres, as the explosiveness of hydrogen that can be stored in one micro sphere is bearing vanishingly small safety hazards. Solid hydrogen storage requires temperatures below 14 Kelvin. Hence, hydrogen is stored reversibly in these four different ways either by absorption, which means that the hydrogen molecules are chemically bonded to the storage material or by adsorption, where the molecules maintain their physical forms and are just trapped in the potential minimum of the surface of the storage material.

There exist a number of hybrid solutions, such as the cryo-compressed tank that

combines cryogenic temperatures with high pressures that aim to overcome the disadvantages of two storage methods. For instance the hybrid solution of chemical storage in $NaBH_4$ and physical storage in hollow glass micro spheres that is the topic of this thesis, solves some of the issues of both systems. By using this hybrid system, costs can be notably reduced, while the volumetric storage density of hollow glass micro spheres can be increased. Remaining problems are the needed repeated recyclability of the spheres and the required high temperature over a period of time long enough for the gaseous hydrogen to leave the spheres [7].

2.2 Hollow Glass Micro Spheres

Storing hydrogen in hollow glass micro spheres (HGMS) bears the main advantage of security, as they are non-explosive because of the small amount of hydrogen that is released in case of a malfunction of a sphere. The diffusivity of hydrogen through glass is highly temperature dependent, meaning that hydrogen is only diffusing through glass at high temperatures (250 ° C – 400 ° C), over a certain activation energy barrier. That temperature dependence is utilised for the storage of hydrogen in glass spheres. Hydrogen is loaded into the spheres at elevated temperatures, then the system is cooled down to room temperature which locks the hydrogen molecules inside the spheres as the glass is no longer permeable for hydrogen molecules, which stores them inside the spheres. For unloading, the spheres are heated again to above 250 ° C.

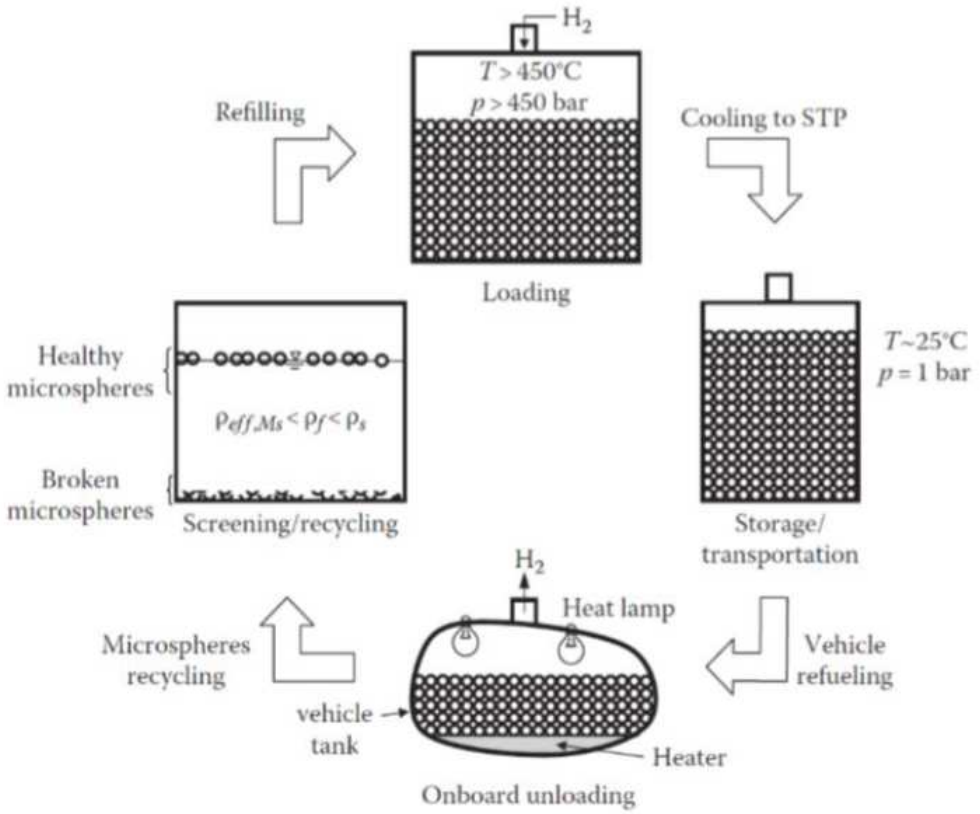

Figure 2.2: Life cycle of a HGMS, taken from [29]

The technology was first proposed by Teitel in 1980 [30]. He combined the hydrogen storage in hollow glass micro spheres with a metal hydride system that increases the volumetric storage density of the storage system. Desirable properties of the hollow glass micro spheres are high diffusivity at corresponding loading and unloading temperatures, as well as chemical and thermal durability [31]. The durability of the HGMS is of great importance, as the spheres have to be reused in order to minimise costs. Hence, after the spheres are unloaded and the hydrogen is used for energy generation, the spheres are washed with a hydrochloric acid (HCl) and distilled water mix (two parts of water with one part of HCl). This changes the pH-value of the HGMS from alkaline to neutral (pH-value of 7). During the washing process the

broken HGMS are separated from the intact spheres. The intact spheres are then loaded again. The whole HGMS cycle from the loading to the unloading, washing and re-loading process of the HGMS can be seen in figure 2.2. As the hollow glass micro spheres act as small pressure vessels for the hydrogen, the spheres must be build in a way that withholds the outer pressure of 85 MPa in the loading process. The spheres need to be of a size that is big enough to exhibit a volumetric storage density that makes it competitive with other storage techniques. At the same time, a bigger sphere size requires a thicker shell, which reduces the diffusion rate of hydrogen through the glass shell and minimises efficiency. In other words, the size – shell thickness ratio of the spheres need to be optimised to enhance the efficiency of the storage system.

Within the framework of this thesis $3M^{TM}$ micro spheres of the type S38 are used. They hold pressures of up to 100 MPa, have an average diameter of 28 μm, a sphere shell thickness of 2 μm, a softening point at 600°C, a packing factor of about 60% and a gravimetric storage density of 8,46%. Therefore, the maximum amount of hydrogen that can be loaded into one gramm of HGMS is 0,0846 g. The material with which the HGMS are fabricated with, is soda-lime-borosilicate-glass [32]. The spheres are loaded with a pressure of 85 MPa and a temperature of 523 K (250 °C). Thus, the extraction temperature should be close to 523 K also.

2.2.1 Fabrication Process of HGMS

There are well established fabrication processes of hollow glass micro spheres (HGMS). According to Qi et al. [31] the most common production technology is flame sprayed pyrolysis. Another method is called liquid droplet method.

Flame Spray Pyrolysis

Firstly, glass frits are produced by crushing glass. As the glass shreds are of different sizes after they are produced, the glass frits are then sieved to be of uniform size. The glass frits contain a blowing agent (e.g. sulphate, urea) and are sprayed through an oxyacetylene flame that reaches temperatures between 1000 °C and 1200 °C. The blowing agent decomposes at elevated temperatures and leaves a cavitation bubble inside the spheres behind. The process is visualised in figure 2.3.

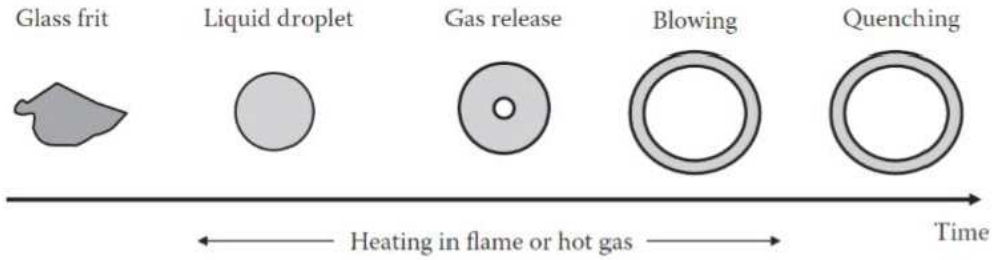

Figure 2.3: Development of a glass shard throughout the process of flame spray pyrolysis. Taken from [29]

Liquid Droplet Method

Within this technique liquid-based droplet containing glass-formations fall through a vertical drop tower furnace, with different temperature regions. The droplets are generated by dissolving glass-forming components in an aqueous solution and transported by a controlled air flow that passes through the tower, from top to bottom. The temperature in the furnace rises as the droplet falls. In the first region of the drop tower, the water from the surface of the droplet evaporates at moderate temperatures. An elastic gel membrane encapsulating the rest of the droplet remains. Secondly, the water from inside the membrane evaporates and diffuses through the membrane to dry out the shells. This second region leads to solid gel particles. Region number three is responsible for the transition from gel particles to glass spheres

as this is where the density of the spheres is increased. After that, the residual gases are released from inside the shell in region number four. Lastly, the uniformly shaped spheres are shock-refrigerated in the collection area, as visible in figure 2.4 [29]. The initial source material, the aqueous solution, allows only a very limited choice of glass compositions, which makes it difficult to modify the sphere properties such as the shell strength or permeability by adding elements to the system [31].

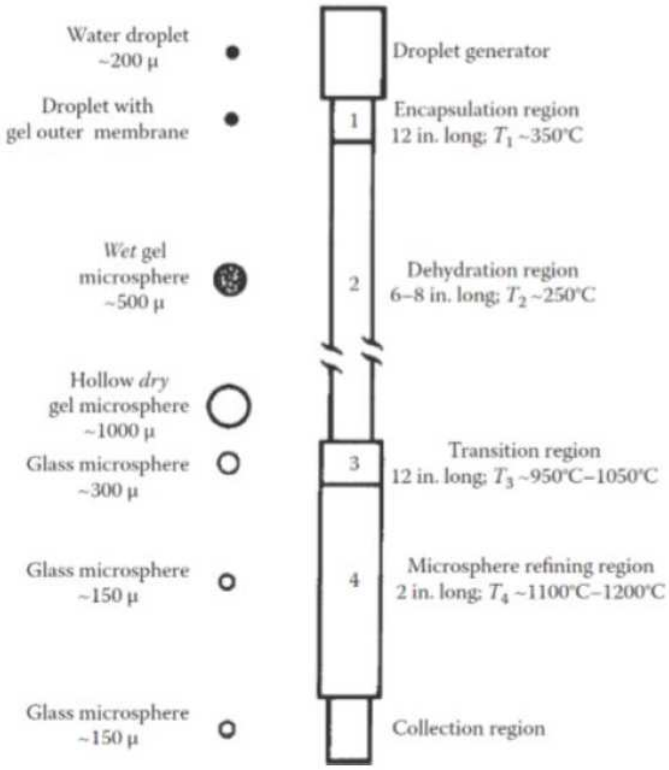

Figure 2.4: Production of HGMS in a drop tower furnace. Taken from [29]

Qi et. al. [31] use a dried gel method, which is a method that uses a drop tower furnace. The initial material is a gel made from metal alkoxides with 8 wt% water and 5 wt% urea [33]. The gel is then dried, crushed and sieved before it goes through the furnace. This method shows nearly no limits to the source material, which makes it suitable for the modification of sphere properties.

2.2.2 Storage Capacities of HGMS

As the experiments within this thesis are executed with unloaded HGMS, meaning HGMS with no hydrogen inside, the amount of hydrogen that would theoretically leave the spheres, hence the theoretical hydrogen yield, is calculated.

As mentioned before, glass diffusivity is highly dependent on the ambient temperature. Hydrogen is loaded into micro spheres by heating the spheres up to 250 – 400 °C and applying pressure of about 85 MPa. At these conditions, the surrounding hydrogen diffuses into the spheres. In other words, the hydrogen is pressed into the spheres. Once the hydrogen is in the spheres, the system is cooled down to room temperature where the sphere walls are no longer permeable to the hydrogen which is then locked inside the spheres. To release the hydrogen the spheres need to be heated up again to 250 – 400 °C.

The theoretical hydrogen storage capacity can be calculated by taking a look at the pressure function inside the spheres that is dependent on the permeability of the micro spheres. The permeability is dependent on the diffusion and the chemical reaction of hydrogen with glass. As part of the hydrogen initially loaded into the spheres chemically reacts with the sphere shells, the chemical reaction of hydrogen with glass is limiting the diffusion process while unloading the hydrogen from the micro spheres. Reactions of hydrogen with the glass shells may include reduction of ions like Fe^{3+} or Sn^{4+} to form OH groups. Hence, not all of the hydrogen loaded into the spheres can be unloaded due to a chemical reaction of glass with hydrogen. However, within this theoretical calculation the chemical reaction will be neglected. Below 100 MPa the permeability is not dependent on pressure. Therefore the permeability K(T) for systems with pressures lower than 100 MPa is given by

$$K(T) = K_{norm} T e^{-Q_k/T} \tag{2.1}$$

The activation energy Q_k is a constant and K_{norm} is a normalisation factor. Their values can be found in table 2.1. Both constants are extracted from [7]. The time dependent pressure p(t) inside the spheres is given by

$$p(t) = p_{amb} + (p_{HGMS} - p_{amb})e^{-Ct} \tag{2.2}$$

$$C = K(T)\frac{3RT}{d \cdot r} \tag{2.3}$$

which is derived from the ideal gas equation. p_{HGMS} is the pressure inside the spheres after unloading and C is the diffusion rate that measures the diffusion of hydrogen out of the HGMS per second. As the pressure inside the spheres decreases continually while the hypothetically loaded hydrogen leaves the spheres, an iterative approach was chosen. Meaning, the pressure inside the spheres p_{HGMS}, is not constant throughout the process.

$$K_i = K_{norm}T_i e^{-Q_k/T_i} \tag{2.4}$$

$$C_i = K_i\frac{3RT_i}{d \cdot r} \tag{2.5}$$

$$p_i = p_{amb} + (p_{i-1} - p_{amb})e^{-C_i \cdot t_i} \tag{2.6}$$

$$1 \leq i \leq 12631$$

Permeability K_{norm} [mol/(Pa m s)]	$2{,}787 \cdot 10^{-17}$
Gasconstant R [kg m^2 /(s^2 mol K)]	8,314
Activation Energy Q_K [K]	4026
Ambient Pressure p_{amb} [Pa]	101325
HMGS Wallthickness d [μm]	0,75
HMGS Radius r [μm]	1

Table 2.1: Used constants.

During one hydrolysis experiment that lasts one hour, 12631 data points are collected. Therefore, the iteration has 12631 steps. After every step, the temperature, the permeability, the diffusion rate and the pressure inside the spheres changes. The specific temperature profile is either taken from experimental data or from hypothetical temperature curves that simulate experimental data. The initial pressure inside the spheres p_0, which is the starting point for the iteration, can be calculated with the loading (B_L) and extraction (B_E) coefficient that have been extracted from literature [34].

$$B_L = \frac{B_1}{T_L} + \frac{B_2}{T_L^2} \tag{2.7}$$

$$B_E = \frac{B_1}{T_0} + \frac{B_2}{T_0^2} \tag{2.8}$$

$$p_0 = \frac{p_L T_0}{T_L(1 + B_L p_L) - B_E p_L T_0} \tag{2.9}$$

p_0 is the initial pressure in the spheres and T_0 is the initial temperature in the reaction chamber. All values to be inserted into equations 2.1 - 2.11 can be found in tables 2.1 - 2.3 The amount of the decrease in pressure inside the spheres divided by the temperature inside the reaction chamber, is then summarised and multiplied by a constant factor, to obtain the amount of hydrogen that would leave the spheres throughout the whole hydrolytic reaction.

$$n(t) = \sum_i (p_{i-1} - p_i) \frac{V \cdot M_{H2}}{R \cdot T_i} \tag{2.10}$$

Ambient Pressure p_{amb} [Pa]	101325
Loading Pressure p_L [Mpa]	85
B_1 (taken from [34])	$2{,}01 \cdot 10^{-6}$
B_2 (taken from [34])	$-5 \cdot 10^{-7}$
Loading Temperature T_L [K]	523
Extraction Temperature T_0 [K]	300
Molar weight of H_2 M_{H2} [g/mol]	2,02

Table 2.2: Used constants.

The maximum storage capacity of one HGMS is described by the gravimetric storage density, which is the weight of the hydrogen that can be stored in the HGMS, compared to the weight of the unloaded HGMS. With the gravimetric storage density, the maximum amount of hydrogen of one hydrolytic reaction can be easily calculated.

$$m_{max} = m_{HGMS} \cdot \gamma_G \tag{2.11}$$

HMGS mass for one reaction m_{HGMS} [g]	0,8
Gravimetric Storage Capacity γ_G [%]	8,457

Table 2.3: Used constants.

Considering that the mass of the HGMS required for one reaction is 0,8 g and the gravimetric storage density is 8,457 %, the maximum hydrogen storage capacity of one hydrolytic round is 0,068 g.

2.3 A Hybrid Hydrogen Storage Solution: Hydrolysis & HGMS

In this section the hybrid hydrogen storage solution that combines the two storage solutions, hydrolysis of sodium borohydride ($NaBH_4$) with water and HGMS

is described. Hollow glass micro spheres have many advantages such as their high gravimetric storage density and their cheapness compared to other storage systems. However, they also bear disadvantages such as a low volumetric storage density. Also, to release the hydrogen trapped inside the hollow glass micro spheres a temperature of over 250 ° C has to be generated, ideally without consuming a lot of energy and in a reasonable amount of time. To remedy this problem, a hybrid solution, first introduced by Tajmar and Keding in 2008 [35] is proposed, where micro spheres and hydrolytic systems are combined, due to their complementary properties. Hydrolytic systems have a high gravimetric and volumetric storage density, but bear the disadvantage of being very expensive. Hydrides generate high temperatures when the hydrogen is released. Hence, when those two storage systems are combined, the advantages of both techniques can be used to optimise the storage system. The hybrid storage system accounts for reducing costs and enhancing the volumetric storage density. Furthermore, the heat produced by the hydrides can be used to unload the hydrogen molecules that are only released from the spheres when a heat of over 250 °C is applied.

Hydrolysis refers to the hydrolytic reaction that can be described by the reaction equation

$$NaBH_4 + 4H_2O \rightarrow NaB(OH)_4 + 4H_2 + \Delta H^\circ \tag{2.12}$$

where $\Delta H^\circ = -216,8$ kJ/mol is the enthalpy difference which can be calculated from property tables given in CRC Handbook of Chemistry and Physics [36] and can be compared to literature values [37]. The enthalpy difference accounts for the heat released during the hydrolytic reaction that makes the glass spheres permeable for hydrogen molecules.

In the suggested patent by Keding and Tajmar [35], $NaBH_4$ is added to the glass

spheres as a liquid, whereas this thesis uses $NaBH_4$ as a solid, in the shape of fine grained powder.

2.4 Catalyst

A catalyst is a material that influences the speed of a chemical reaction, without being consumed in the process. The catalyst decreases or increases the activation energy of the reaction by building intermediate stages with the reactants. The reaction between the reactants A and B (equation 2.13) would take an activation energy of E_{AB}. A catalyst C reacts with reactant A to build an intermediate stage (equation 2.14). The end product (equation 2.16) is built over a second intermediate stage (equation 2.15). When the activation energy E_{AB} is higher than the activation energies of E_{AK} and E_{AKB}, hence the catalyst decreases the activation energy, it is called a positive catalyst. When E_{AB} is lower than E_{AK} and E_{AKB}, it is called a negative catalyst.

$$A + B \rightarrow AB \tag{2.13}$$

$$A + C \rightarrow AC \tag{2.14}$$

$$AC + B \rightarrow ACB \tag{2.15}$$

$$ACB \rightarrow C + AB \tag{2.16}$$

Therefore, the catalyst increases or decreases the speed of the reaction. Catalysts change the kinetic properties of a chemical reaction without influencing its thermodynamics. Furthermore, catalysts are selective, which means that certain reactions need certain catalysts [38]. Within the framework of this thesis, a positive catalyst is sputtered onto the hollow glass micro spheres to decrease the activation energy of

the reaction taking place between sodium borohydride ($NaBH_4$) and water. Schmid [7], who did pioneer work for the hybrid hydrogen storage of hollow glass micro spheres with pulverised $NaBH_4$, made a thorough evaluation of possible catalysts. Based on an in-depth literature research, he chose a couple of noble metal catalysts. Two materials were chosen: ruthenium (Ru) and platinum (Pt). Experiments proved the ruthenium catalyst to be the most efficient.

2.5 Bonding Agent

Various substances cannot bond well with each other, as the surface potential with its potential bonding sites do not cooperate well with each other. Therefore, a bonding agent that bonds well with both materials is needed in between. For instance, ruthenium and glass do not bond well. Experiments show, that a ruthenium layer on a glass surface can be destroyed and removed with water. Hence, a bonding agent is needed that bonds well with either substance. Furthermore, the efficiency of a catalyst increases with its surface area. Hence, when choosing a bonding agent, its surface area is taken into account. Schmid [7] did in-depth literature research to find a suitable, sputter-able catalyst support material that led him to TiO_2 and Al_2O_3. Since TiO_2 was found to be more commonly used and showed better results, TiO_2 was chosen. Hence, within the framework of this thesis, a ruthenium catalyst with a titanium dioxide support material was sputtered onto the HGMS.

3 Experimental Set-up

This section will describe the different methods used in this thesis. The sputtering process of the catalyst layer will be explained, as well as the experimental set-up for the hydrolysis. The heat of the hydrolytic reaction between sodium borohydride ($NaBH_4$) and distilled water shall be used to extract the hydrogen molecules from the hollow glass microspheres (HGMS), in presence of a catalyst that is sputter-coated onto the HGMS. Furthermore, the microscopes: Digital Viewer GE-5 and Polyvar MET Light, will be discussed. As the catalyst stability is the main limiting factor for re-usability of the HGMS, the microscopes are used to capture the degradation induced upon the catalyst within adhesion tests.

3.1 The Sputtering Process

Within the framework of this thesis, sputtering was used to coat the HGMS with the catalyst layer that enhances the efficiency of the hydrolytic reaction. The method includes the separation of the catalyst material from a source (also called target) that then condenses onto the HGMS.

3.1.1 Sputter Deposition

Sputtering makes use of a working gas, mostly a noble gas such as argon that is fed into a high vacuum chamber with pressures below 0,5 Pa. A voltage between 150 and 3000 V is applied between an anode (substrate) and cathode (target) that

are situated in the high vacuum chamber. Electrons that move from the cathode to the anode ionise the working gas, in this case argon. The positive ions are then attracted by the negatively charged target (cathode). Once the ions reach the target, they separate material from the target by transferring their momentum to the target. As material is ejected from the target in its atomic or molecular form, the target material is transferred from its solid to its gaseous state. The gaseous target material is then condensing onto the substrate material, here the HGMS. The voltage remains constant throughout the whole sputtering process to keep the target under ion bombardment.

The sputtering yield Y is the mean value of the number of atoms that are emitted from the target, per ion that hits the target. Significant factors, which influence Y, are the target material, the type of ions used, the energy and the angle of incidence [39].

3.1.2 Magnetron Sputtering

While conventional sputtering includes only an electrical field, magnetron sputtering implies an additional magnetic field that is oriented parallel to the target, hence orthogonal to the electric field. The magnets that generate the magnetic field (usually permanent magnets with a field strength of about 0,1 T) are situated behind the target with one pole sitting in the middle of the target and the other pole forming a ring around the first pole. The overlapping of the electric and the magnetic field forces the electrons onto a spiral track, due to the Lorentz force. Hence, the path of the electrons between the anode and the cathode is enlarged, which increases the number of collisions per electron and enhances the ionisation rate and therefore the number of ions. Due to the arrangement of the magnets, the electron density is the highest, where the magnetic field lines are parallel to the target surface, hence in between the two poles. As the mass of the ions is too big for them to experience a

significant distraction from their path, the ion bombardment is biggest where the electron density is highest and therefore the erosion of the target is the highest. The advantages of magnetron sputtering are the enhanced sputtering rate and that it can be executed at a lower pressure and voltage at the target, due to the enhanced ionisation rate[7].

3.1.3 Reactive Sputtering and Coating of the Substrate Material

Additionally to the working gas, in this work argon, a reactive gas is added in the process. The reactive gas reacts with the target surface and condenses onto the substrate material to build a reaction layer surface. To avoid poisoning, a careful control of the reactive gas flow is necessary. Further information on reactive sputtering can be found in [40].

For the coating of the HGMS with the TiO_xRu catalyst layer reactive magnetron sputtering was used. As the spheres stick together in vacuum and cannot be coated with the catalyst layer from every side, a tilted rotating vessel (figure 3.1) was implemented by Schmid [7]. This construction agitates the HGMS which keeps them from sticking together and provides for a more uniformly spread catalyst layer on the HGMS.

All coatings were produced in pulsed DC reactive sputtering mode with the sputter source being an Advanced Energy Pinnacle^{TM} Plus + 2x5 kW. The samples produced in this work, were sputter-coated with argon as the process gas and oxygen as a reactive gas. A mass flow controller (MKS Type 1179) kept the argon flow at values to provide an argon pressure of 0,5 Pa. The oxygen flow was adjusted to keep the overall pressure in the chamber at 0,536 Pa. The residual gas was analysed with a quadrupole mass spectrometer. All planar samples as well as the hollow glass microspheres were first coated with the bonding agent titanium-oxide (TiO_x) with a power of 400 W and then with ruthenium (Ru) together with TiO_x at 200 W

each. The sputtering time is calculated with the sputtering rate of the target and the expected layer thickness. The sputtering rate (unit: [m/s]) is determined experimentally by measuring the layer thickness after a certain time. For the sputtering process of the HGMS a medium sized vessel, with a maximum capacity of 100 ml and a tilting angle of 45 ° relative to the vacuum chamber walls (figure 3.1) was used.

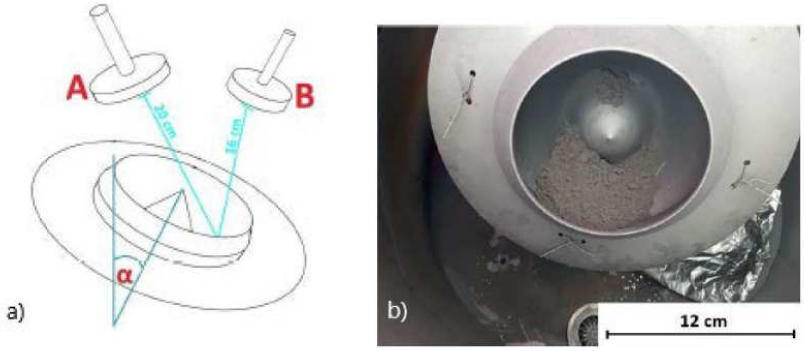

Figure 3.1: a) tilted rotating vessel with the titanium (A) and ruthenium (B) target, $\alpha = 45°$ and b) vessel containing TiO_xRu coated HGMS, taken from [6]

3.2 Hydrolysis Set-up

Figure 3.2 shows the set-up of the hydrolytic reaction experiment. Firstly, the whole set-up, meaning all joints between tubes, funnels and flasks have to be sealed with vacuum sealing-grease to avoid loss of gaseous or liquid matter. The 3000 ml measuring cup (7) on the balance (8) is filled with tap water. A suction tube not visible in the picture is used to suck the water from the measuring cup to the two 1000 ml dropping funnels (6), then the balance is set to tare. 0,81 g HMGS are filled into the three-necked-round-bottom-flask (4) together with 0,81 g $NaBH_4$. The hydrolytic reaction between sodium borohydride ($NaBH_4$) and distilled water starts once the distilled water (4 ml) that is filled into the dropping funnel (5), is led into the 100

ml three-necked-round-bottom-flask by opening the valve between the three-necked-round-bottom-flask (4) and the 50 ml dropping funnel (5). The gaseous hydrogen released, is flowing through the blue tubes to the two 1000 ml dropping funnels (6) and presses the water into the 3000 ml measuring cup (7) on the balance (8). This way the amount of hydrogen released in the reaction is measured by the pressure it exerts on the water, thus by the weight of the water that is forced into the measuring cup.

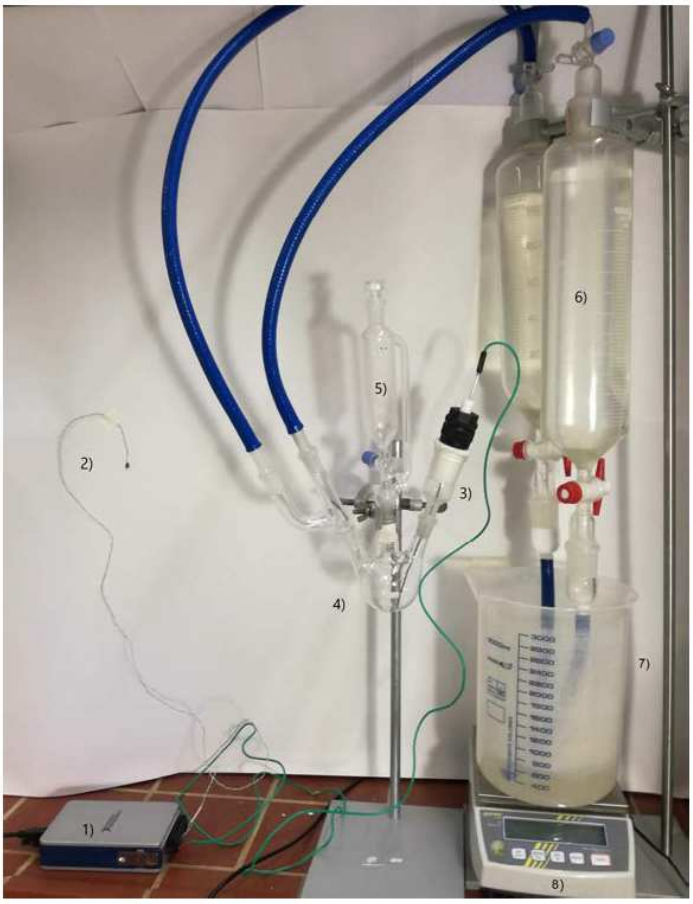

Figure 3.2: The hydrolysis set-up is a home-made construction consisting of 1) a temperature measurement board with 2) an ambient temperature thermometer, 3) a thermo-element, 4) a 100 ml three necked round-bottom-flask, 5) a 50 ml dropping funnel, 6) two 1000 ml dropping funnels, 7) a 3000 ml measuring cub and 8) a balance.

After the hydrolytic reaction the HGMS are washed with distilled water and then with an acidic bath consisting of hydrochloric acid (HCl) and distilled water (two parts of water with one part of HCl). This fulfills the purpose of changing the pH-value of the HGMS from alkaline to neutral (pH-value of 7), which reactivates the catalyst. Also, the washing process separates the broken HGMS from the intact ones. This reduces the amount of spheres notably, which makes it necessary to mix the HGMS of two first hydrolytic cycles to have enough material for the second cycle. The HGMS of two second cycles are then used for a third cycle and so forth. Before the HGMS can be mixed together and reused, the HGMS are dried in a drying chamber at around 100 °C. One hydrolytic cycle means the whole process of the hydrolytic reaction with its follow-up treatment (reactivation of the catalyst and drying of the HGMS).

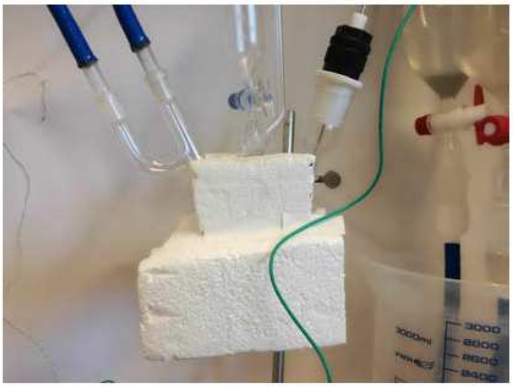

Figure 3.3: To insulate the reaction chamber, the three-necked-round-bottom-flask was insulated with Styrofoam.

The temperature at which the hydrogen would be loaded into the spheres is 250 °C. Therefore, the extraction temperature should be as close to 250 °C as possible. This heat should be provided by the catalytic reaction between sodium borohydride and water. Experiments with 0,81 g of $NaBH_4$, 0,81 g of sputter-coated HGMS and 4 ml of water, lead to peak temperatures of around 90 °C. The amount of hydrogen

that can be loaded into the spheres is 0,066 g. If the temperature is 90 °C at the peak of the reaction, 0,002 g of the loaded hydrogen would leave the spheres during the hydrolytic reaction, hence a percentage of 3% of the initial load. The hydrolytic reaction releases 0,2 g hydrogen approximately. This also means that if the HGMS would be loaded, only about 10% of the hydrogen would come from inside the HGMS. The other 90% would be produced in the reaction. To see how a thermally insulated reaction chamber would affect the temperature curve inside the reaction chamber and subsequently the amount of hydrogen leaving the spheres, a Styrofoam insulation was constructed for the reaction chamber. The Styrofoam insulated three-necked-round-bottom-flask can be seen in figure 3.3.

3.3 Digital Viewer GE-5

The Digital Viewer GE-5 by Aigo is a digital microscope that provides a resolution of 1280 x 1024 pixel, a 1/2" Color CMOS image sensor and a spectrum response between 400 nm - 1000 nm. The samples (coated planar glass substrates) are illuminated by an inbuilt LED. Two different magnifications, 60X and 180X can be chosen. In this experiment the magnification is 60X. The working distance is around 0,8 cm.

As the hydrogen yield weakens after each hydrolytic cycle, detailed experiments were executed, to find out which step of the hydrolytic cycle could be problematic. The different degradation steps executed on the samples, are as follows:

1. Exposure to humidity (water)
2. Catalysis of the hydrolytic reaction between $NaBH_4$ and distilled water
3. Reactivation of the catalyst (exposure to a hydrochloric acid - water mixture)

The Digital Viewer GE-5 offers the advantage of having an easily accessible and removable sample holder (figure 3.4) on which the sample can be affixed to. This makes it possible to execute the degradation experiments without having to remove

the sample from the sample holder in between the different degradation steps. Therefore, pictures can be taken while the degradation experiment is running. This makes it easier to see the effect of the treatment as a constant position can be maintained during the degradation procedure. However, during the experiment it turned out that in some cases, it was not possible to observe the same spot throughout the different steps of the destruction experiment, because the water, $NaBH_4$ powder or hydrochloric acid (HCl) - water mixture could not always be reliably positioned on the same spot on the coated planar glass substrate. Another limiting factor of the experimental set-up is that during the hydrolytic reaction small droplets hit the lens which blurs the picture. Therefore, only the pictures before and after the hydrolytic reactions could be used and the lens had to be cleaned in between. The illumination can be varied between top, bottom or top and bottom illumination. As the catalyst layer is highly reflective, it is challenging to capture all samples using the same illumination settings. The quality of the Digital Viewer GE-5 is not sufficient to compensate this. Therefore, the illumination was varied on each sample, to portray the catalyst layers in the best possible way. Hence, the catalyst layer color is not uniform on all images.

Figure 3.4: Digital Viewer GE-5 where 1) is the removable sample holder [41]

3.4 Reichert Polyvar MET Light Microscope

The Polyvar MET Light microscope (figure 3.5) is an optical microscope constructed by the Reichert Division of the Leica corporation. The adjusting stage with the sample holder is stepper motor driven in x and y directions, with a step size of 0,5 μm. The maximum stage travel is 100 x 100 mm. The stage is manually height-adjustable. The resolution of the digital camera mounted on the microscope is 2048 x 1536 pixel [42]. There are five objective lenses between 5X and 150X magnification. The eyepiece has a magnification of 10X and can be zoomed in by factors of 0,8X, 1X and 1,25X. For this work a 5X magnification was used with an eyepiece multiplication factor of 1,25X, which leads to a total magnification of 62,5 ($5 \cdot 10 \cdot 1{,}25$) The working distance was less than 0,5 cm. In contrast to the Digital Viewer GE-5, the Polyvar MET Light microscope does not have an easily accessible sample holder that allows for execution of the degradation experiments while the sample remains on the sample holder. But as the degradation steps could not be captured during the degradation itself with the Digital Viewer GE-5 anyways, the Polyvar MET Light microscope was used for further investigations, as it has higher resolution. Bottom illumination by a high power LED lamp, with a voltage of about 32 V was used for all pictures. Therefore, the color of the catalyst is uniform on every picture.

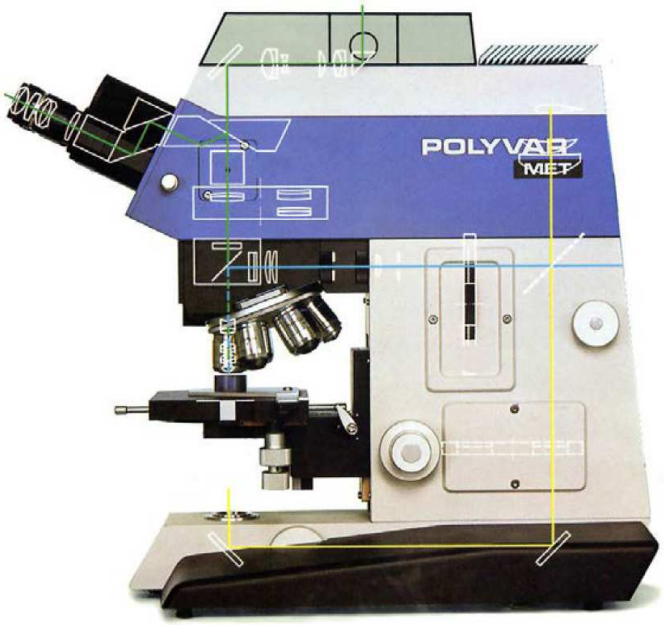

Figure 3.5: Polyvar MET Light microscope with the paths of the light beam marked on the picture [42]

4 Results & Discussion

This chapter is divided into three subsections. Firstly, the hydrolysis was performed with unfilled hollow glass micro spheres (HGMS), to ensure reproducibility of the predecessors work [6, 7]. Performing hydrolysis with unfilled HGMS sets the focus on the durability of the catalyst layer and the performance of the chemical reaction between sodium borohydride and water that generates hydrogen. Secondly, different thicknesses of the bonding agent are sputtered onto planar glass substrates. The substrates are then destroyed in the same fashion as the hydrolysis would do, to see the effect of the thickness of the bonding agent on the durability of the catalyst layer. At last, a theoretical calculation and evaluation of the hydrogen loading and de-loading process of the spheres was made, to find optimum parameters for future experiments with loaded microspheres.

4.1 Hydrolysis of HGMS coated with a catalyst layer

The purpose of this experiment was to reproduce the previous work [6, 7] and to validate the method used that includes hydrolysis of sputter-coated HGMS with sodium borohydride and water. The hollow glass microspheres were first coated with the bonding agent titanium-oxide (TiO_x) with a power of 400 W and then with ruthenium (Ru) together with TiO_x at 200 W each. The catalyst layer as well as the bonding agent were affixed onto the HGMS with reactive magnetron sputtering (section 3.1.2). A detailed overview of the parameters used for the sputtering process

can be found in the set-up chapter 3. The set-up of the hydrolysis experiment can be found in section 3.2. In this section the hydrolysis of two different samples will be discussed. Both samples were sputter-coated with a 0,5 nm TiO_x (bonding agent) layer and a 10 nm TiO_xRu (catalyst) layer (figure 4.1).

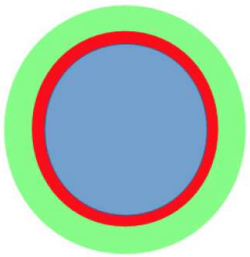

Figure 4.1: Schematic illustration of a catalyst (green) sputter-coated HGMS (blue) with its bonding agent (red); layer thickness not to scale

4.1.1 Sample 01

As the HGMS gain efficiency with respect to their storage capability with every time the HGMS can be reused, the aim was to increase the number of hydrolytic reactions executed with the same set of HGMS. To reuse the HGMS, the catalyst has to be reactivated. For this purpose the HGMS are washed with distilled water and then reactivated in an acidic bath consisting of hydrochloric acid (HCl) and distilled water (two parts of water with one part of HCl). This changes the pH-value of the HGMS from alkaline to neutral (pH-value of 7). During the washing process, the broken hollow glass microspheres are separated from the intact spheres. This reduces the amount of spheres notably, which makes it necessary to mix the HGMS of two first reactions to have enough material for the second reaction. The HGMS of two second reactions are then used for a third reaction and so forth.

The first sample of HGMS was sputter-coated with a bonding agent and catalyst layer and examined for its durability. Thus, the first sample of sputter-coated

HGMS was used for several hydrolytic reactions. The whole set-up of the experiment, including the composition of the catalyst thin-film and the parameters of the sputtering process of the TiO_xRu, is the same as in [6, 7]. Table 4.1 gives an overview of the sputtering parameters. The results, as given in figure 4.2, show that only three hydrolytic reactions worked. It is fair to assume that the catalyst layer wore off after the third reaction.

Process Gas	Argon
Argon Pressure	0,5 Pa
Reactive Gas	Oxygen
Oxygen Pressure	0,036 Pa
Bonding Agent	TiO_x
Power TiO_x	400 W
TiO_x Thickness	0,5 nm
Catalyst	TiO_x Ru
Power TiO_x	200 W
Power Ru	200 W
TiO_x Ru Thickness	10 nm

Table 4.1: Coating Parameters

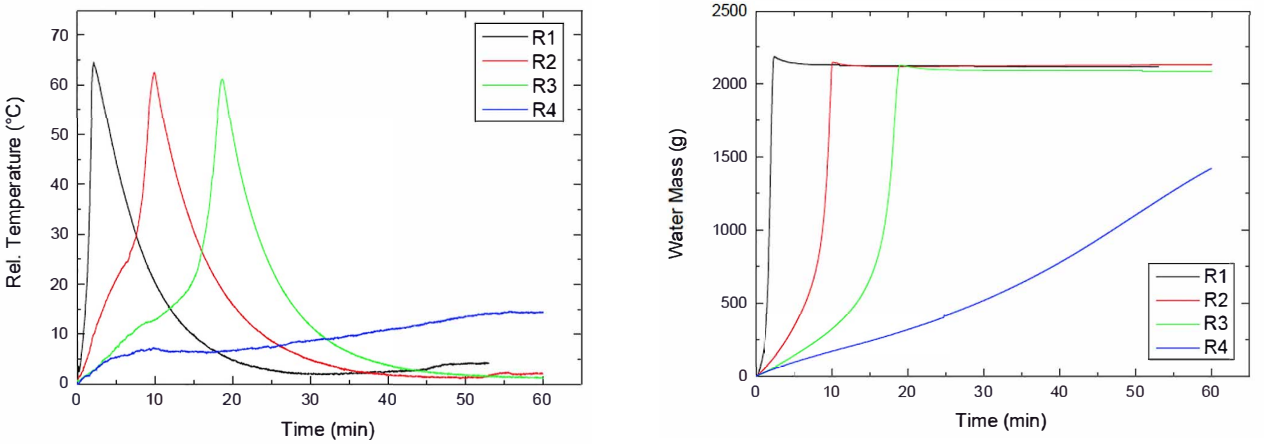

(a) Relative temperature progression

(b) Mass curve

Figure 4.2: Acquired during the hydrolysis reaction between $NaBH_4$ and water in the presence of a TiO_xRu catalyst. The reactions, executed one after the other, are labelled with R1-R4.

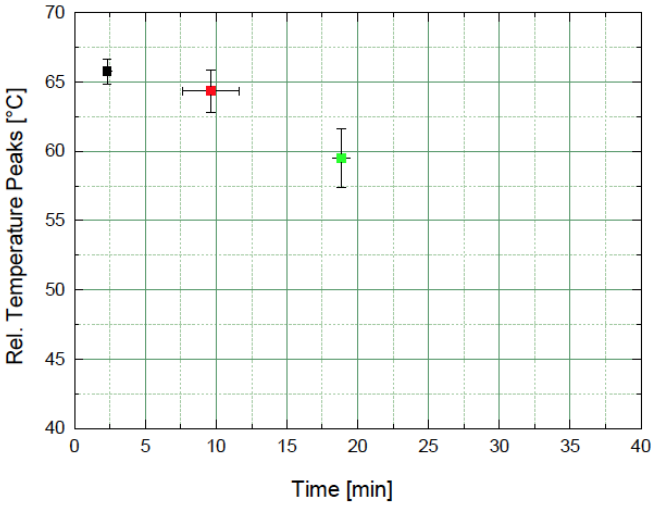

(a) Relative temperature peaks

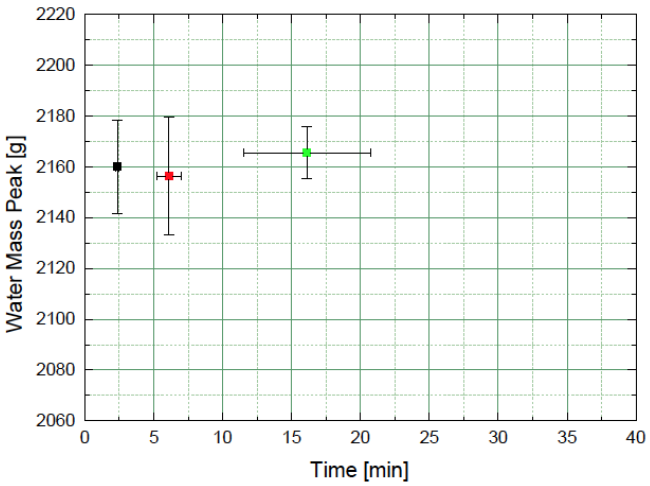

(b) Total hydrogen mass; y-axis value taken from minute 50, x-axis value taken from 4.2.b.

Figure 4.3: Obtained from figure 4.2.

As already explained, the amount of HGMS is notably reduced at each hydrolytic round, which makes it necessary to mix two first rounds to have enough material for a second round. Hence, eight first reactions are necessary to ultimately have enough material for a fourth round. To have enough material for a hypothetical fifth round, twelve first reactions were made. Figure 4.2 shows exemplary temperature and water mass curves of one first, second, third and fourth hydrolytic round. The error bars of figure 4.3 show the deviations of all hydrolytic reactions of one round, so the deviations of the mean value of all twelve first reactions, six second reactions, three third reactions and one fourth reaction. It would be possible to make two fourth reactions out of three third reactions, as the loss of HGMS decreases after every hydrolytic round. But as the fourth reaction did not work out, meaning that it did not show the typical temperature peak like the first three reactions, no further reactions were made. Figure 4.2.a shows the relative temperature, i.e. the temperature of the reaction minus the ambient temperature of the room, of all four

hydrolytic reactions. The first reaction has a peak of 64.13 °C, after 18 minutes and 58 seconds. The peak temperature of each reaction then decreases linearly and equidistantly, meaning that the time lapses in between the peaks are constant, as visible in figure 4.3. The water mass (figure 4.2.b) first increases sharply with the increasing temperature of the reaction, reaches a peak and then stays constant in good approximation, after the reaction subsides. The temperature increases just as sharp as the water mass and peaks when the reaction is completed. Then the reaction chamber cools down gradually. When the reaction chamber cools down, the hydrogen in the reaction chamber cools down as well which increases its density and decreases its volume. Therefore, the water mass decreases slightly after it reaches its peak. The peak of the water mass is taken at room temperature, hence when the reaction has cooled off, i.e. at minute 50. The water mass peaks around 30 seconds behind the temperature peak (figure 4.3). That is due to the set-up, which is in a way that the hydrogen passes approximately 50 cm long tubes until it reaches the balance (section 3.2). The fourth hydrolytic reaction does not show a temperature peak typical for the hydrolytic reaction and the water mass increases steadily in contrast to reactions 1-3, which show a peak in accordance to the temperature peak.

4.1.2 Sample 02

The second sample of HGMS was sputter-coated with the same set of parameters as the first one.

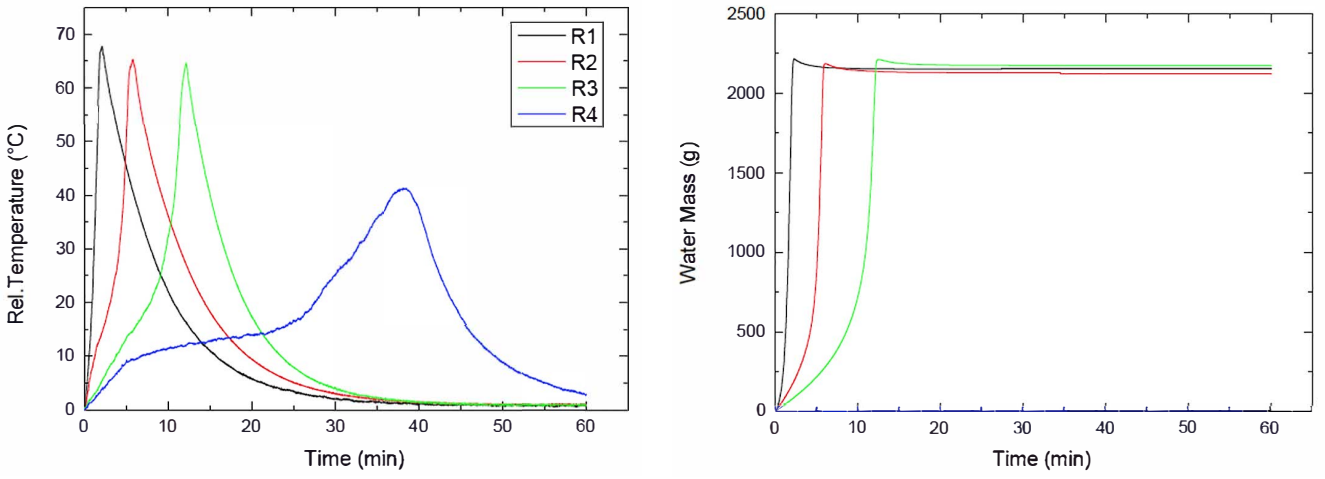

(a) Relative temperature progression (b) Mass curve

Figure 4.4: Acquired during the hydrolysis reaction between $NaBH_4$ and water in the presence of a TiO_xRu catalyst. The reactions executed one after the other, are labelled with R1-R4.

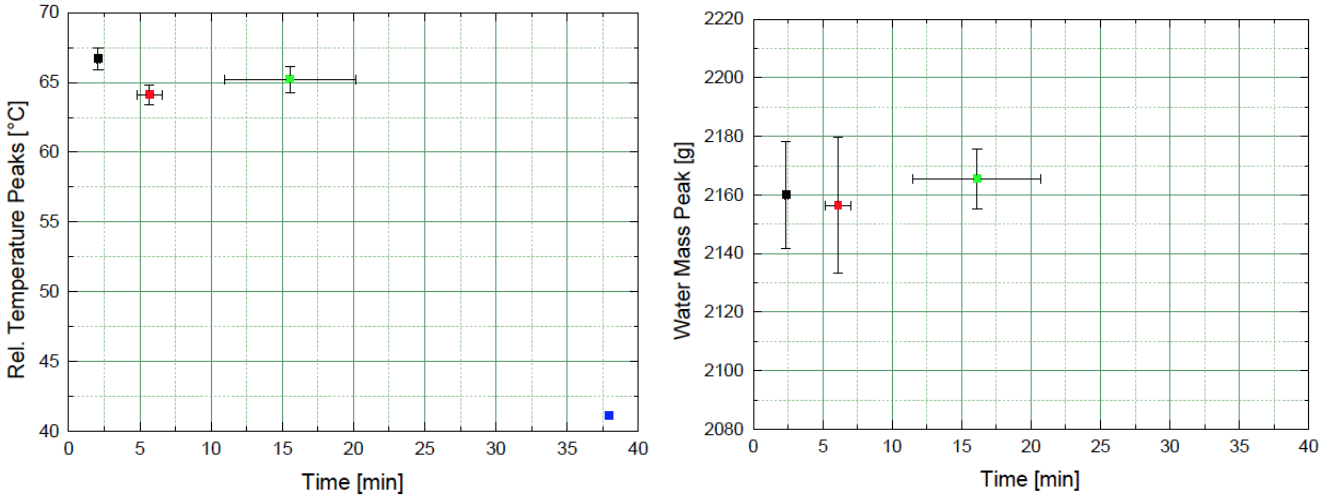

(a) Relative temperature peaks (b) Total hydrogen mass

Figure 4.5: Obtained from figure 4.4

Even though the first three hydrolytic reactions do not differ largely from the results of sample 01, the fourth reaction still exhibits the temperature peak typical

for hydrolysis (figure 4.4). However, the peak is significantly shifted towards later time and the temperature maximum is lower. The data of the total water mass acquired during the fourth hydrolytic reaction could not be collected, due to failure of the balance.

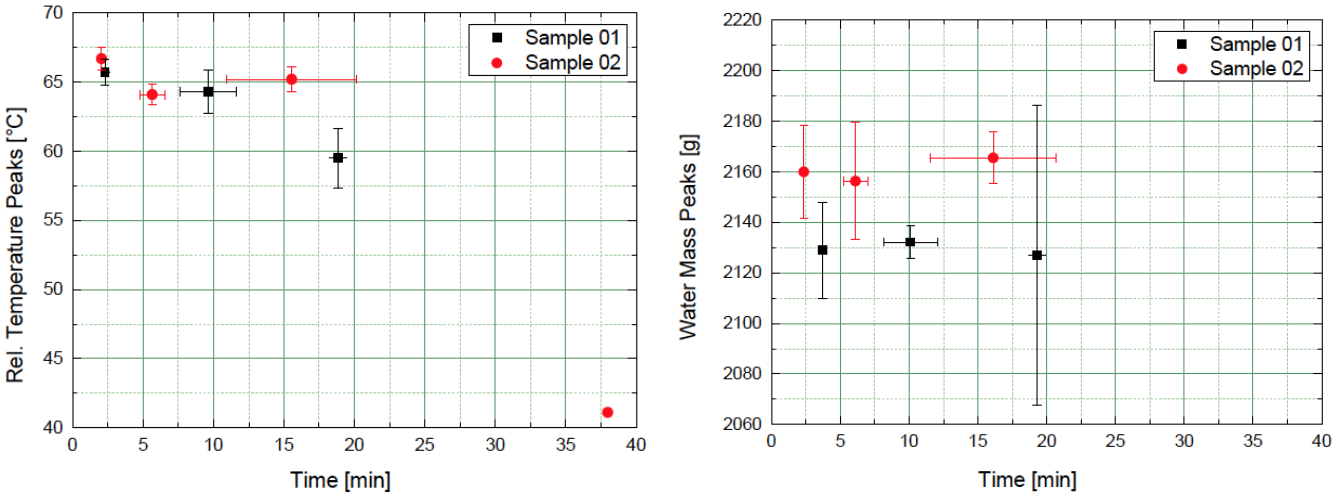

(a) Relative temperature peaks

(b) Total hydrogen mass

Figure 4.6: Obtained from figure 4.4

As Fig.4.6 shows, sample 01 and sample 02 are similarly stable until the third round, meaning that the firth three rounds have similar maximum temperatures.They are all between 59 and 67 °C. Sample 02 is slightly more stable then sample 01, as the first three temperature peaks have more similar values than the temperature peaks of sample 01. The temperature peaks of sample 01 are all between 64 and 67 °C. The hydrogen yield of both samples of the three first rounds are very similar to each other, even though sample 02 has a higher hydrogen yield all in all.

Figure 4.7 shows the originally dark-grey, sputter-coated HGMS as they get lighter after every hydrolytic reaction until they are almost white after the fourth hydrolytic reaction, which is the color of uncoated HGMS.

Figure 4.7: The originally dark-grey, sputter-coated HGMS get lighter after every hydrolytic reaction until they are almost white, which is the color of uncoated HGMS.

Thus, the conclusion that the catalyst wears off after every hydrolytic reaction, reducing the efficiency of the reaction until a reaction cannot be accomplished any more, is evident. Hence, it is fair to conclude that the reason for the hydrolysis to stop working after the fourth reaction is that there is no more catalyst on the HGMS to increase the speed of the reaction. For this reasons, experiments on the degradation of the catalyst layers during the hydrolytic cycle were made, in a simplified arrangement on plane glass substrates.

4.2 Destruction Experiments

4.2.1 Destruction Experiments using the Digital Viewer GE-5

As the resilience of the TiO_xRu layer is key to enable multiple hydrolysis executions, experiments were carried out on that matter. Possible causes for the removal of the TiO_xRu layer could be the exposure to humidity, the reaction with $NaBH_4$ itself or the hydrochloric acid (HCl) bath that is performed to reactivate the HGMS

after every hydrolytic reaction. The water-sodium borohydride ratio, as well as the hydrochloric acid – water ratio is scaled down to fit the scope of the experiment, meaning that 0,5 ml of water is added to 0,1 g of $NaBH_4$ and 0,5 ml were taken out of a hydrochloric acid - water mixture. However, as the hydrolytic reaction is limited by the amount of water added to $NaBH_4$, the exactness of the amount of $NaBH_4$ is not of great importance. Nonetheless, it was taken into consideration that excess water could decrease the reaction temperature and influence the degree of destruction on the catalyst layer. While the titanium-oxide is binding the ruthenium to the surface of the HGMS, the ruthenium is catalysing the reaction. Hence, different bonding agent (TiO_x) thicknesses were tested, while the catalyst layer (TiO_xRu) is 10 nm on every sample, as this is the thickness of ruthenium on the HGMS. The catalyst with its bonding agent is sputtered onto a planar glass substrate, inside the sputter chamber with the glass substrate mounted onto a long substrate holder. Ten samples with different thicknesses of TiO_x (0 nm, 0.15 nm, 0,5 nm, 1 nm, 2 nm, 5 nm, 10 nm, 50 nm, 100 nm) and a constant Ruthenium thickness of 10 nm were produced. The samples were each first exposed to distilled water, then the same samples take part in the reaction between distilled water and $NaBH_4$ and lastly they were exposed to an acid bath. All three destruction experiments simulate one hydrolytic cycle. The destruction is observed and documented with a digital viewer GE-5 microscope. The original aim of this experiment was to take continuous pictures of the reaction, while the reaction takes place, to get a microscopic view on when the destruction takes place in the hydrolytic cycle. In the course of the experiment it turned out that the reaction hazes the lens of the instrument. Considering additionally that the quality of the digital viewer GE-5 is of such that the lighting cannot be set to be equal for every picture, also due to the reflective nature of the surface of the ruthenium layer, the results were used as a pre-examination, to choose three thicknesses (0,5 nm TiO_x, 10 nm TiO_x, 100 nm TiO_x) for further investigations.

Figure 4.8 illustrates how the three different destruction steps influence a TiO_xRu layer for the sample with a 2 nm TiO_x layer. It is visible that water does not influence the durability of the catalyst layer.

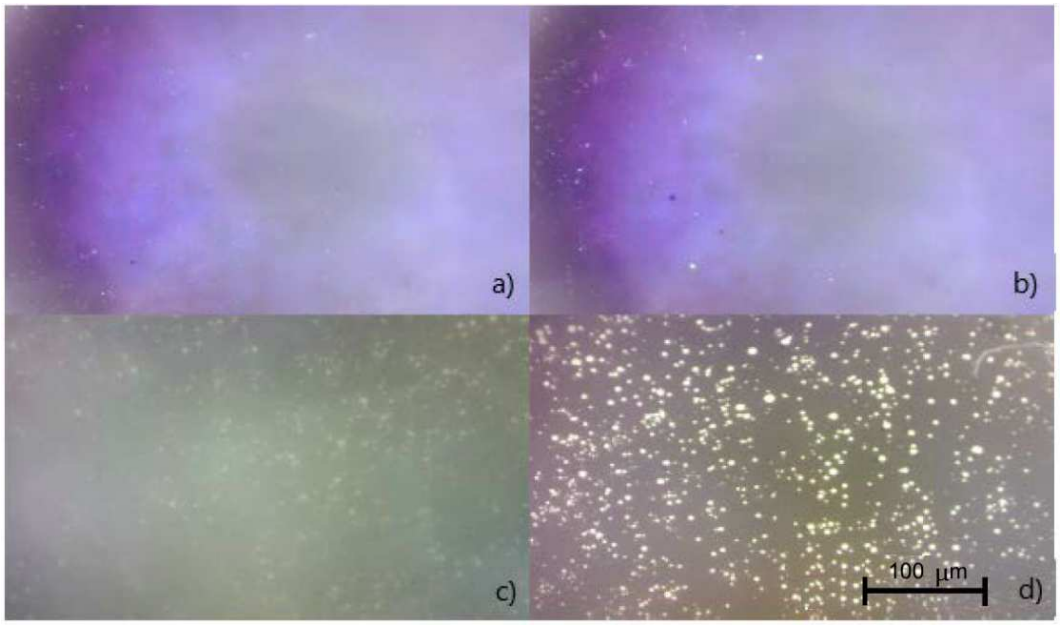

Figure 4.8: TiO_x: 0,5 nm, Ru: 10 nm; The figure shows the sample a) undisturbed b) after water exposure c) after the hydrolytic reaction between $NaBH_4$ and water and d) after hydrochloric acid plus water exposure.

To quantify the percentage of the initial layer remaining on the glass substrate after destruction, the image processing software imageJ was used. Figure 4.9 shows how the software imageJ was used to process the pictures. The threshold adjustment 4.9.c) was completed by visually inspecting the residual layer of the sample.

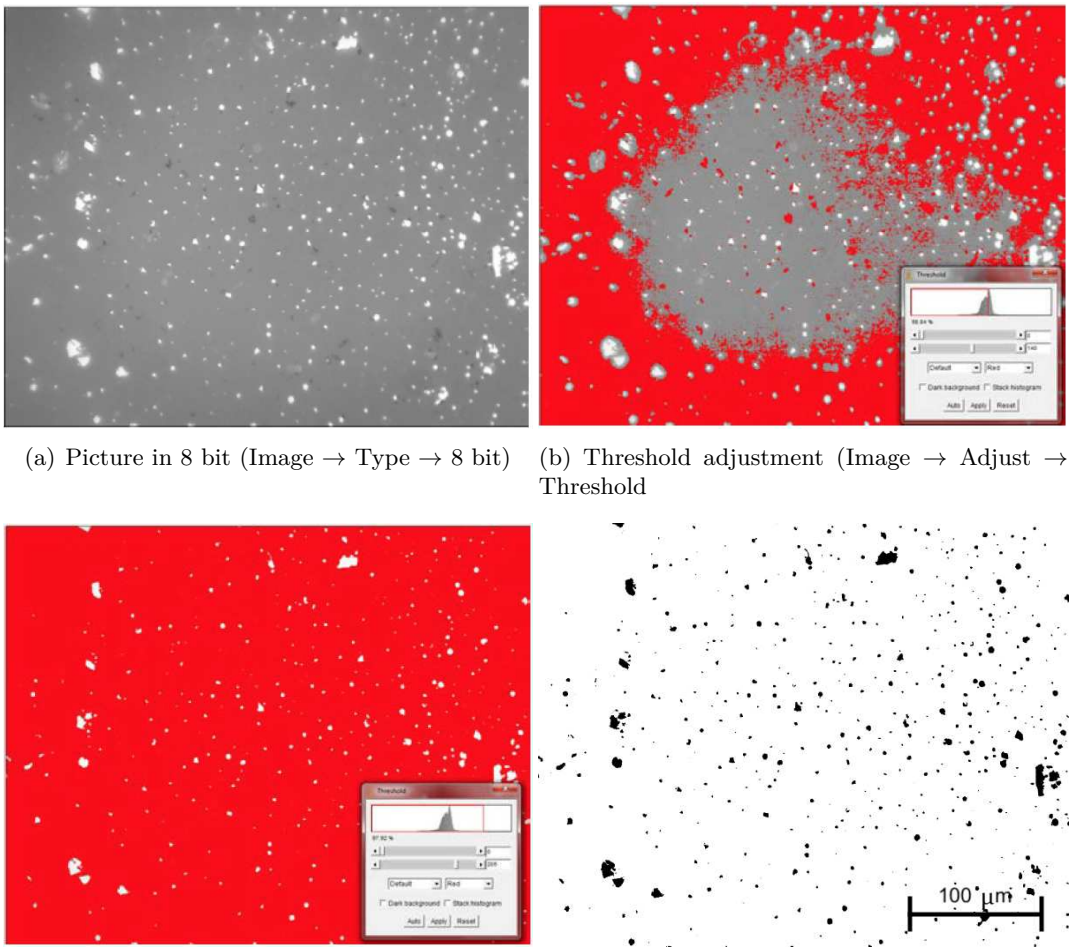

(a) Picture in 8 bit (Image → Type → 8 bit)

(b) Threshold adjustment (Image → Adjust → Threshold

(c) Adjust Threshold until red covers residual layer completely.

(d) Measure area of holes in percent and pixel (Apply (double-click) → Analyze → Analyze Particles → tick boxes: Clear results, Summarize and Include holes → Ok)

Figure 4.9: Step by step guide to quantify residual layer on samples.

The experiments showed that the thin films of the samples with 0 nm and 0.15 nm TiO_x (figures 4.10.a-.b) crack within the first minutes of the hydrolytic reaction and then slowly get washed away as the reaction progresses. The HCl then cleaned the glass of the last shreds of the catalyst layer. The first significant difference in the durability of the catalyst layer appears on the 0,5 nm TiO_x layer (figure 4.10.c). The catalyst layer mostly stays on the glass substrate after the reaction and the

hydrochloric acid – water bath except for some holes. This sample has the same TiO_x and Ru thickness as the HGMS used in experiment 4.1. The sample shown in figure 4.10.g (TiOx: 10 nm, TiOxRu: 10nm), shows a significant difference to the previous ones (figures 4.10.c-.f), as there are notably less holes in the catalyst layer. Hence, the samples with the 10 nm, 50 nm and 100 nm TiO_x layer show the best durability results. As these destruction experiments served as a pre-examination of a quantitative examination, all samples were compared regarding the degree of destruction induced upon them (figure 4.10). It is visible that the catalyst layer on samples 4.10.a-.b is completely gone, 4.10.c-.f has holes in it and 4.10.g-.i is intact. Comparing the nine samples with varying TiO_x layer thicknesses was the basis for deciding to make further quantitative experiments on the 0,5 nm TiO_x, the 10 nm TiO_x and the 100 nm TiO_x samples.

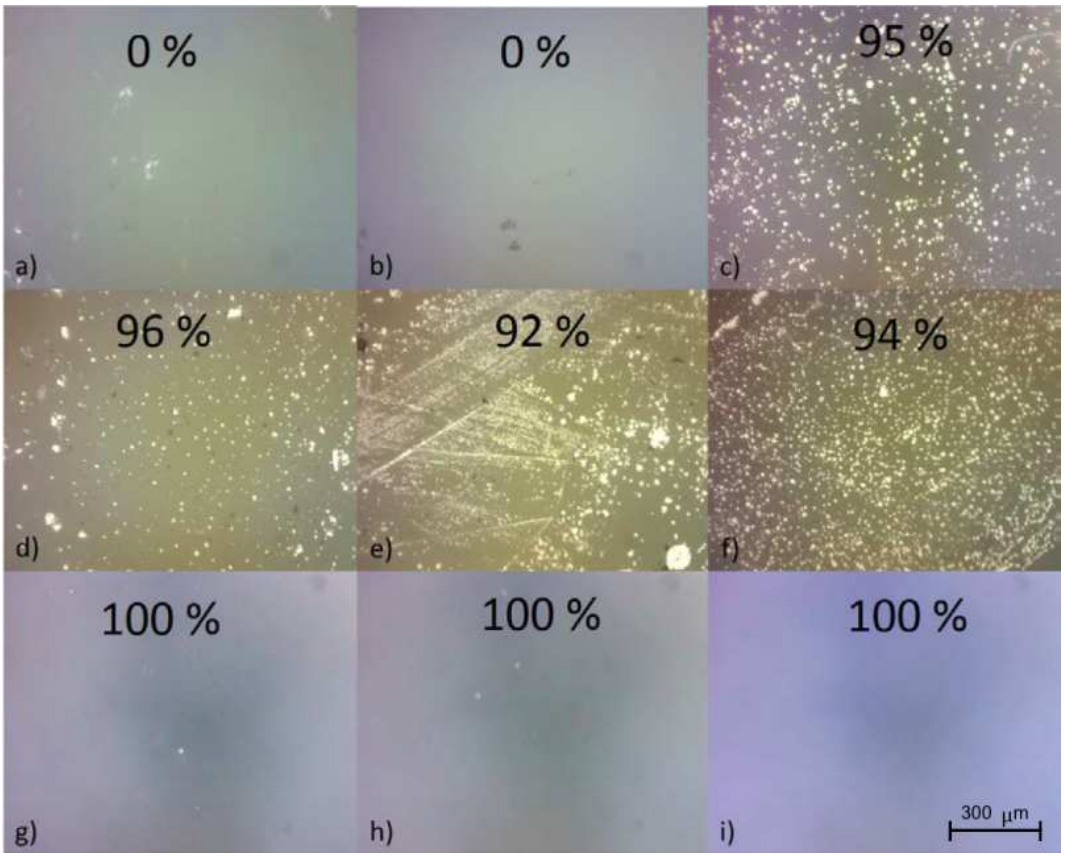

Figure 4.10: This figure shows all nine samples. The percentage in the picture indicates how much of the initial layer is still on the glass substrate after exposure to water, the hydrolytic reaction between $NaBH_4$ and water and hydrochloric acid. a) 0nm, b) 0,15 nm, c) 0,5 nm, d) 1 nm, e) 2 nm, f) 5 nm, g) 10 nm, h) 50 nm i) 100 nm TiO_x

Figure 4.11 visualises the different degrees of destruction on the nine samples with different bonding agent thicknesses. It is apparent that above a TiO_x layer thickness of 0,5 nm, the catalyst has a residual layer percentage of about 90 %. Below 0,5 nm, it can be assumed that the bonding agent thin film is consisting of isles and is not a fully developed continuous layer. It can be concluded that this is the reason why these thin films are less stable and the catalyst layer is easily removed.

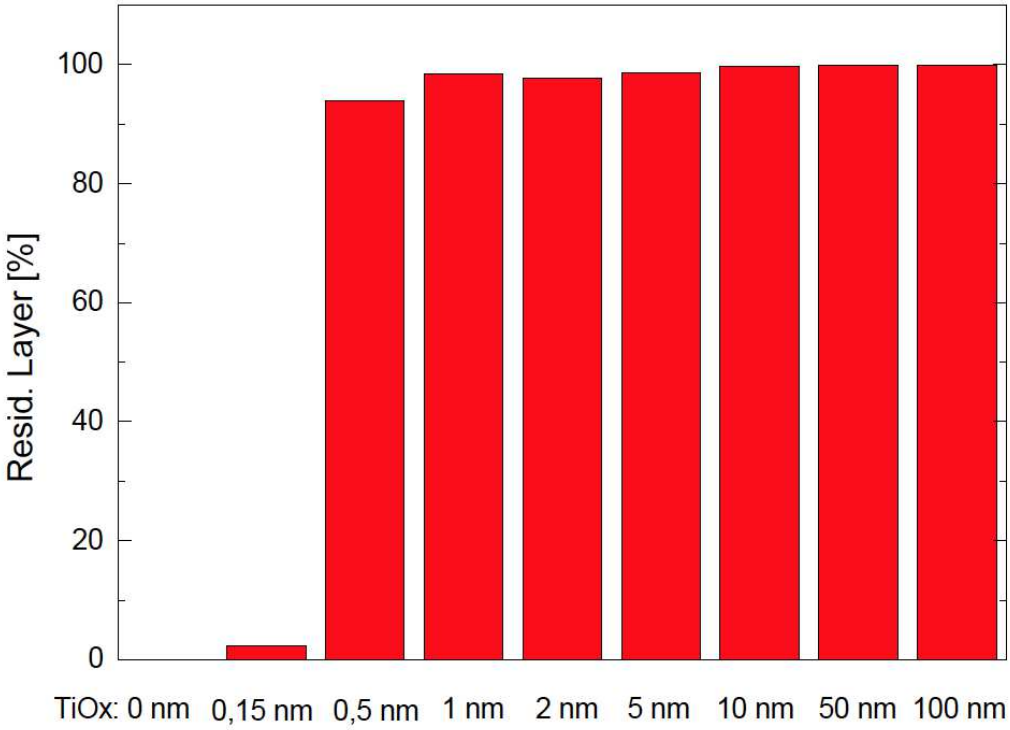

Figure 4.11: Percentage of the residual layer after destruction of all nine samples.

4.2.2 Destruction Experiments using the Polyvar Met Light Microscope

Further destruction experiments were executed with the Polyvar Met Light Microscope using the 5X magnification and a multiplication factor of 12,5X. For this purpose planar glass substrates were sputter-coated with a 0,5 nm, 10 nm and 100 nm TiO_x layer (bonding agent) and 10 nm TiO_xRu (catalyst) layer. The reasons for choosing those three thicknesses are as follows: 0,5 nm is the TiO_x thickness on the HGMS, 10 nm and 100 nm are two different thicknesses that showed a durability of 100 %. Each of those three samples were fabricated five times, to account for the effect of small, inevitable variations of parameters, such as cleanliness of the sample before sputtering that affect the stability of the catalytic TiO_xRu layer. As water did not show any affect on the catalyst layer, the destruction steps included

only the hydrolytic reaction between $NaBH_4$ and water and the hydrochloric acid - water bath. The fact that water does not affect the stability of the catalyst layer is backed by the residual layer percentage after water influence, which is 100 % for each sample. Figure 4.12 illustrates the two destruction steps at the example of a sample with a 0,5 nm bonding agent layer and 10 nm catalyst layer.

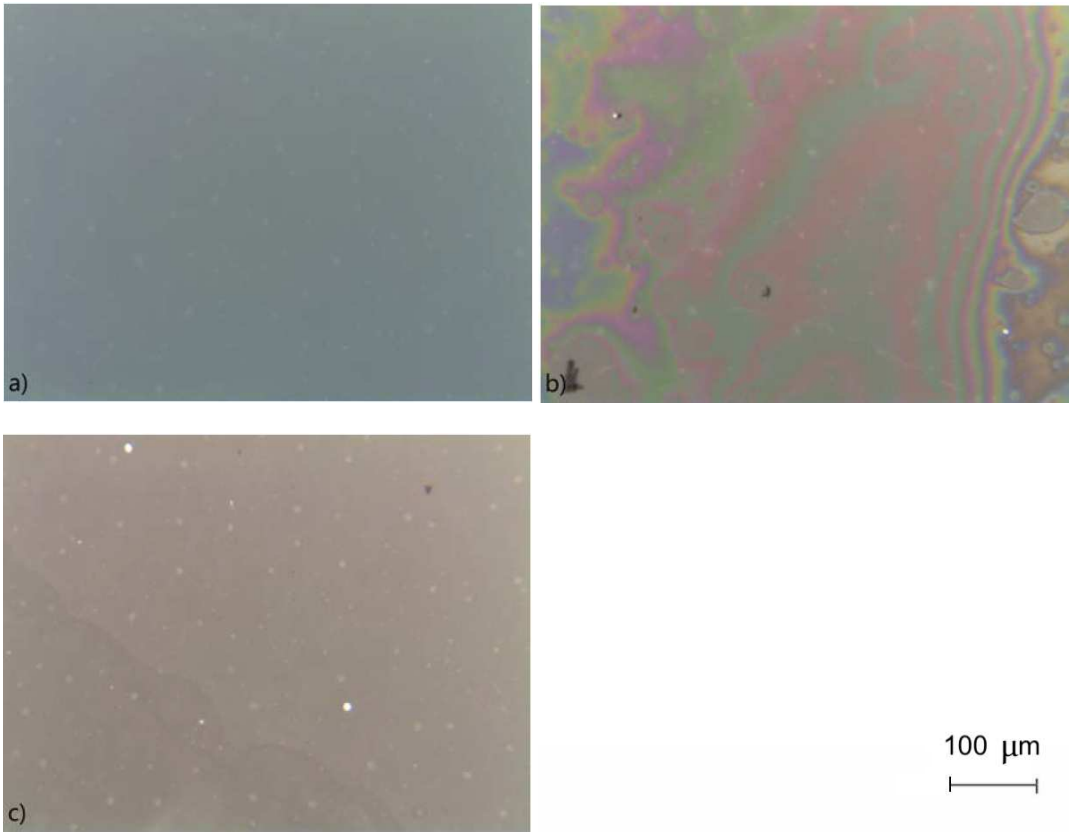

Figure 4.12: TiO_x: 0,5 nm, Ru: 10nm; This figure shows the sample a) undisturbed, b) after the hydrolytic reaction between $NaBH_4$ and water and c) after hydrochloric acid plus water exposure.

A comparison between all samples with the 0,5 nm TiO_x bonding agent, after the hydrolytic cycle, can be seen in figure 4.13. One out of five samples is destroyed after the destruction experiments (figure 4.16). As five samples were made to account for small inevitable variations of parameters such as the cleanliness of the substrate

before sputtering, only the intact samples were used for the analysis of the remaining layer percentage. It is safe to say that a 0,5 nm TiO_x layer is rather consisting of isles of TiO_x than a homogeneously spread thin film. This means that there is a bigger surface area, which is advantageous for the catalyst layer, as the TiO_xRu has more reaction sites available.

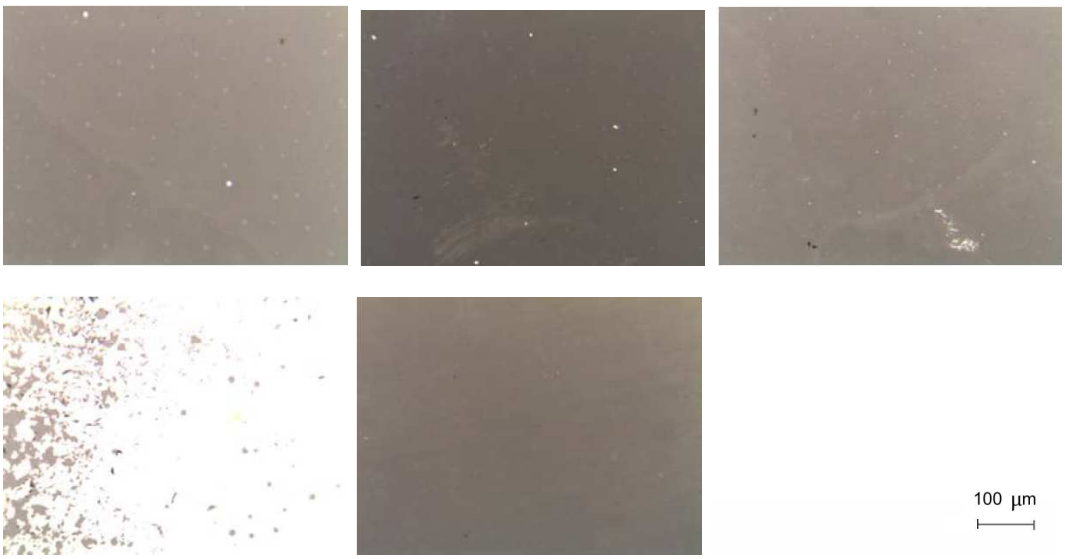

Figure 4.13: TiO_x: 0,5 nm, Ru: 10 nm; All five samples with a 0,5 nm TiO_x layer after the hydrolytic reaction and the exposure to hydrochloric acid.

The catalyst layer samples with the 10 nm TiO_x layer are visible in figure 4.14. Out of five samples three samples are still intact after the destruction experiments (figure 4.16). A 10 nm TiO_x layer is already a homogeneously spread thin film.

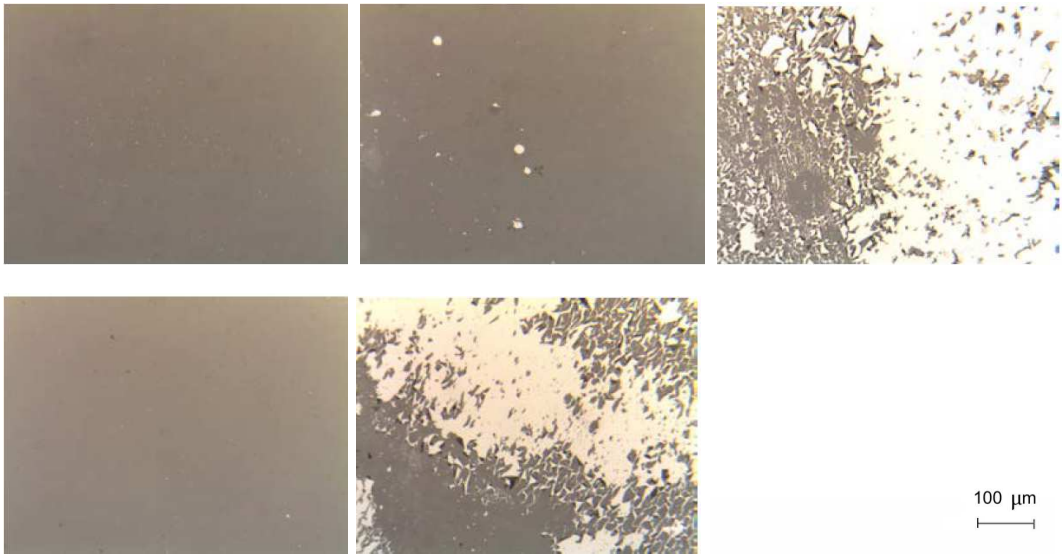

Figure 4.14: TiO_x: 10 nm, Ru: 10nm; All samples with a 10 nm TiO_x layer after the hydrolytic reaction and the exposure to hydrochloric acid.

The 100 nm TiO_x layer samples are visible in figure 4.15. Four out of five catalyst layers are still intact after the destruction experiments (figure 4.16).

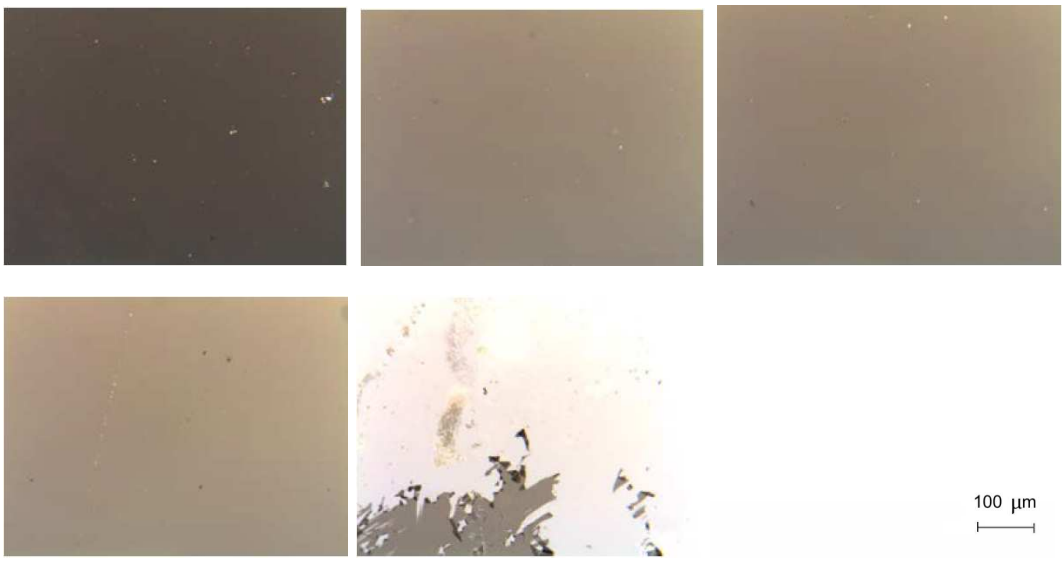

Figure 4.15: TiO_x: 100 nm, Ru: 10nm; All samples with a 100 nm TiO_x layer after the hydrolytic reaction and the exposure to hydrochloric acid.

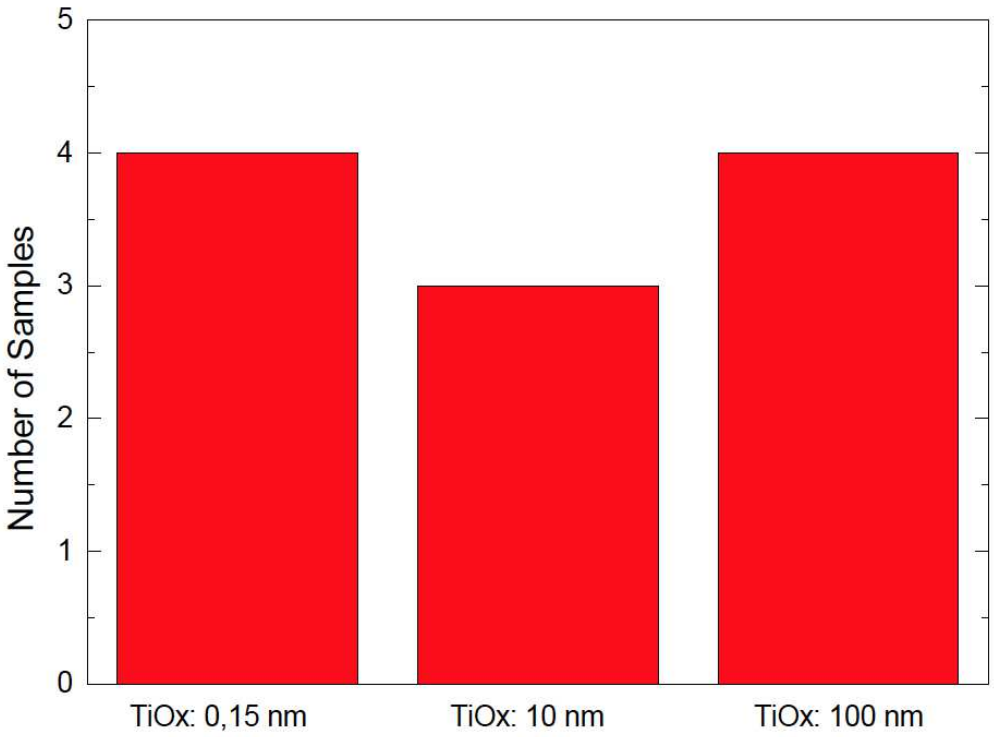

Figure 4.16: Number of intact samples after the destruction experiments, which is also the number of samples used for the calculations of the residual layer percentages of the samples.

Figures 4.17 and 4.18 show the percentage of the mean residual layer of all samples with the same thickness, after the hydrolytic reaction and the reactivation of the catalyst respectively. The durability of all samples is similar, even though the durability of the 0,5 nm and the 100 nm samples appears to be slightly better. The residual layer evaluations have been performed with imageJ, as described in figure 4.9.

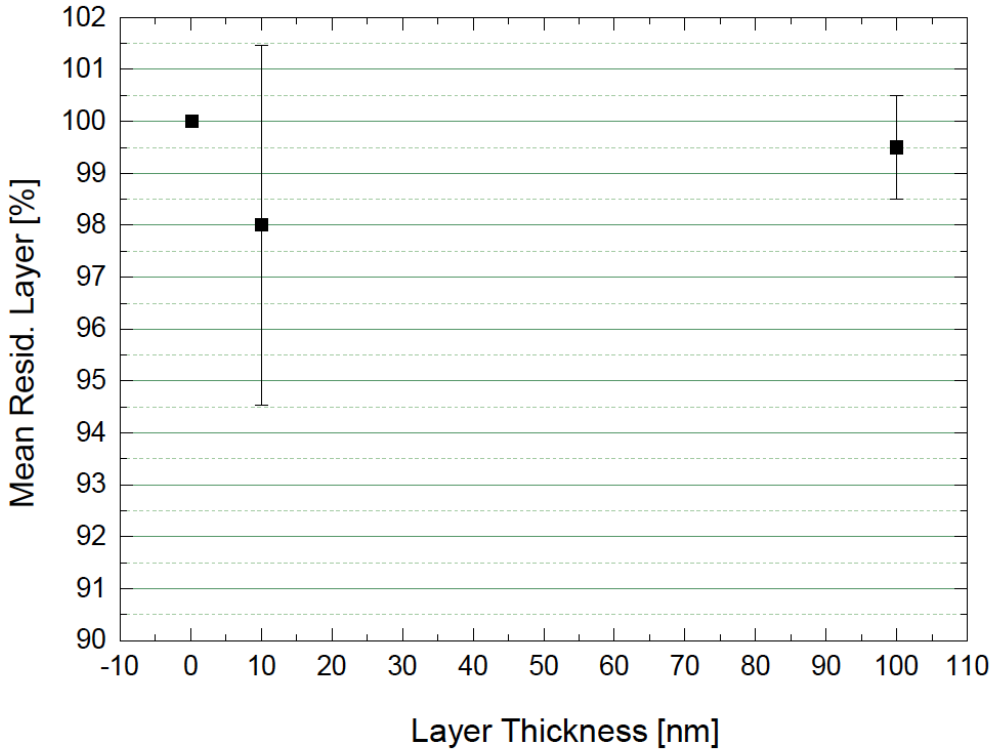

Figure 4.17: Mean residual layer percentage of the samples with the same TiO_x thickness, after the $NaBH_4$ - water reaction with the standard deviation. All four 0,5 nm TiO_x samples have a residual layer of 100%, therefore there is no error bar.

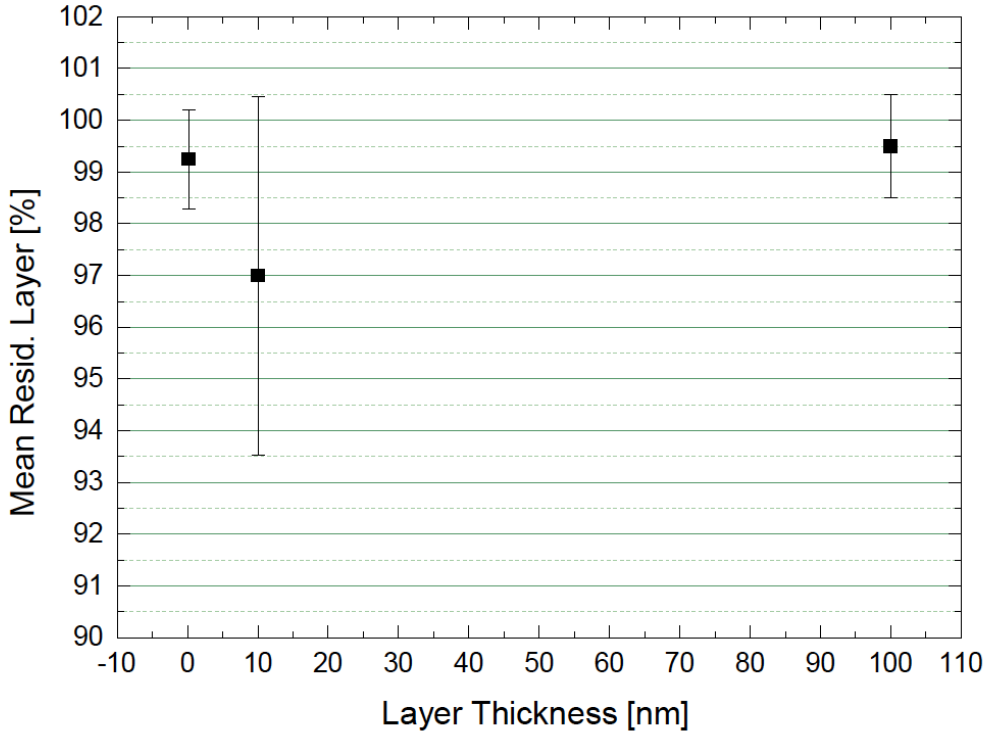

Figure 4.18: Mean residual layer percentage of the samples with the same TiO_x thickness, after the HCl - water bath with the standard deviation.

Comparing the decrease of the residual layer percentage after the hydrolytic reaction and the hydrochloric acid - water bath shows that the residual layer percentage decreases by about 1 % for the 0,5 nm and the 10 nm TiO_x sample, whereas the 100 nm TiO_x sample remains unaffected after both destruction steps (figure 4.19).

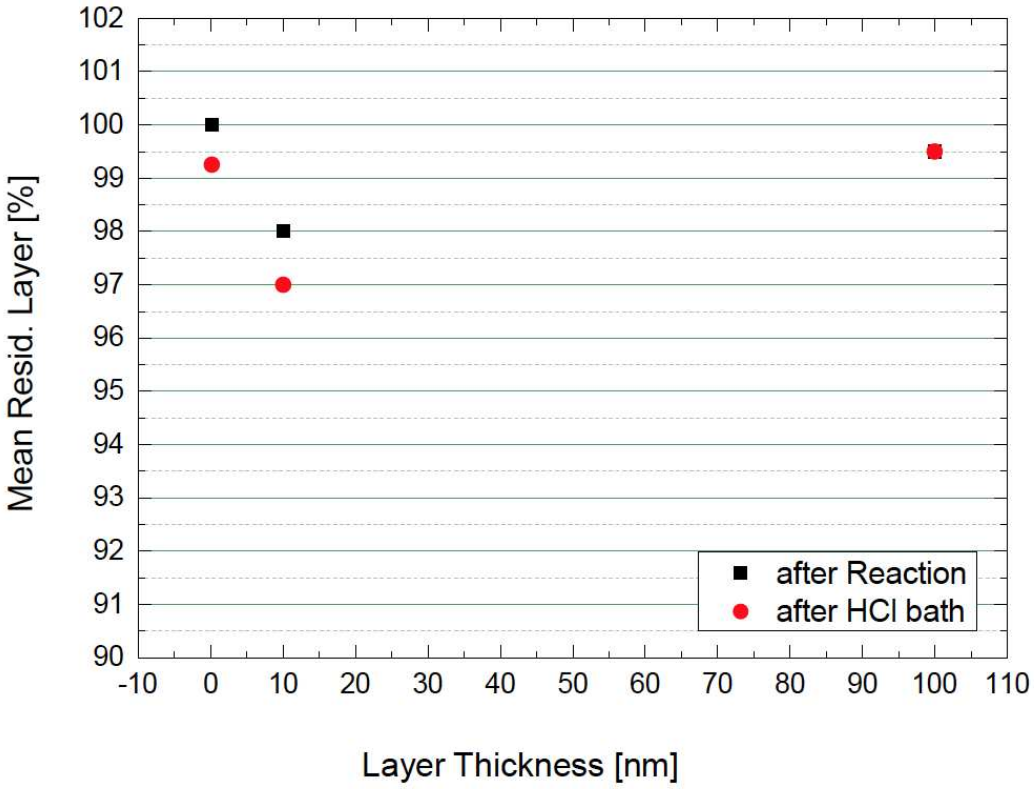

Figure 4.19: Comparison of the destruction after the hydrolytic reaction and after the hydrochloric acid - water bath.

Hence, all three samples (0,5 nm, 10 nm, 100 nm TiO_x) show similar destruction patterns. It shows that a minimum bonding agent thickness of 0,5 nm is required. A thickness above 0,5 nm has no significant effect on the stability of the catalyst layer.

The purpose of the destruction experiments is to find out which step of the hydrolytic cycle causes the destruction. All twenty samples, so all nine samples from the destruction experiments with the Digital Viewer GE-5 and all eleven samples from the experiments with the Polyvar Met Light Microscope, were carefully examined. Of the nine samples from the experiments with the Digital Viewer GE-5, two already got destroyed after the hydrolytic reaction. Therefore there was no layer left for the hydrochloric acid to destroy. Hence, these two samples with a 0 nm and 0,15

nm bonding agent, do not allow a statement concerning the effect of the reactivation process on the layer stability. Therefore, these two samples were not considered in the following examinations, which leaves a total of eighteen samples to observe. Figures 4.20 and 4.21 show what number of samples experience what percentage of depletion due to the hydrolytic reaction and due to the reactivation of the catalyst layer, so the hydrochloric acid.

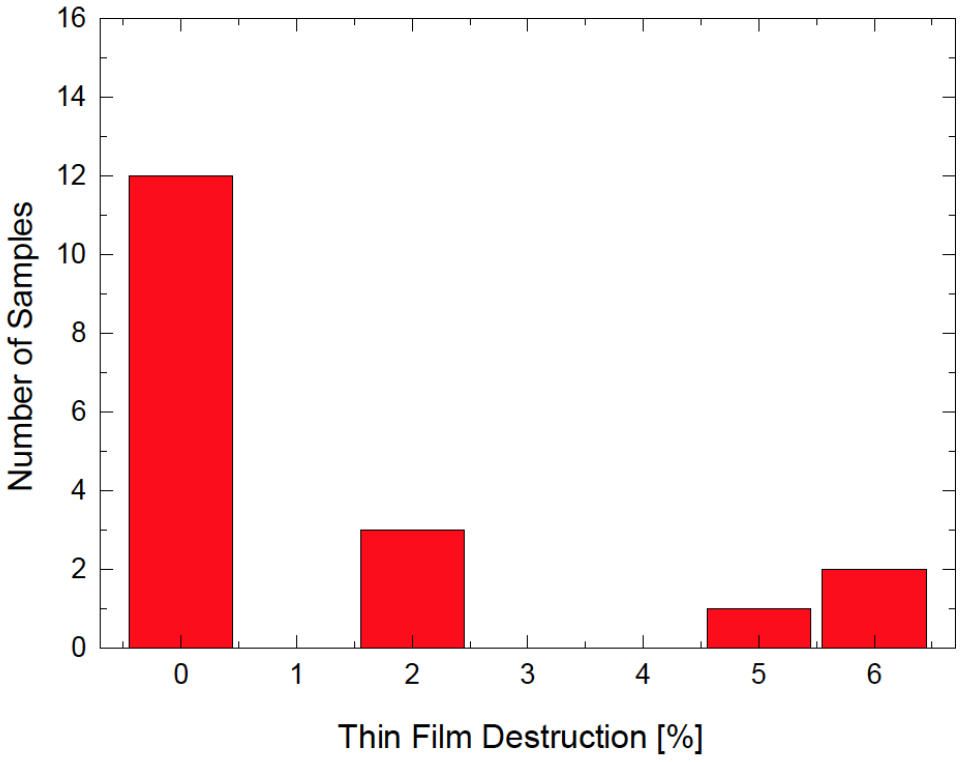

Figure 4.20: Number of samples plotted against the percentage of the destruction of the layer. Twelve samples are not affected by the hydrolytic reaction and six samples are.

All in all, 25% (2·6+5+2·3) of the catalyst layer is removed from all eighteen samples during the hydrolytic reaction.

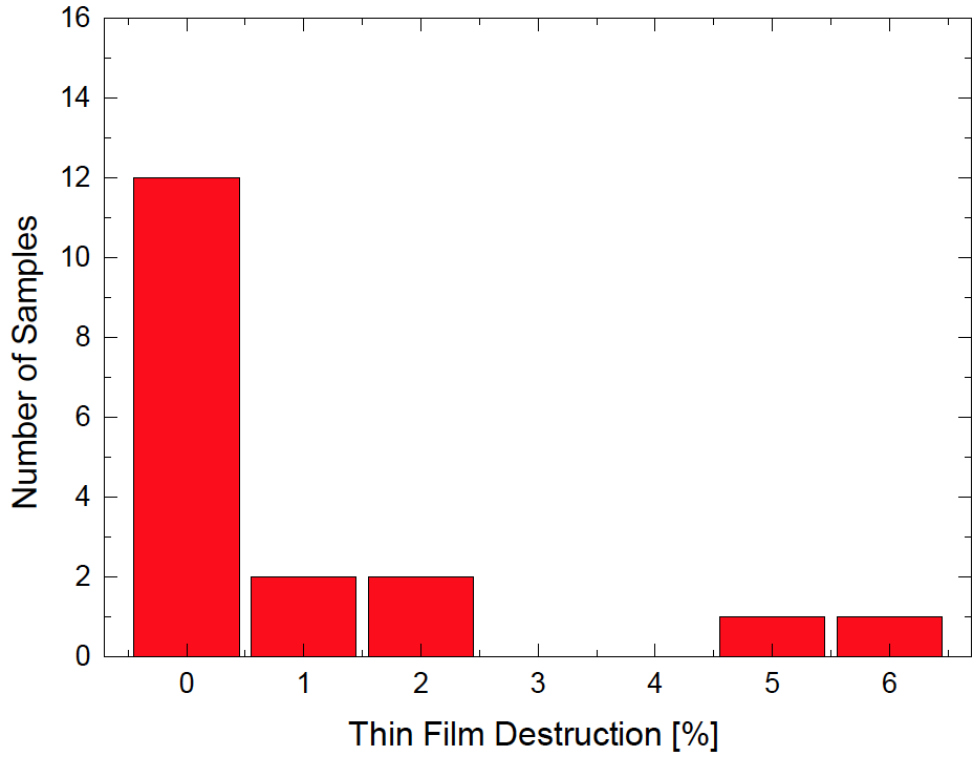

Figure 4.21: Number of samples plotted against the percentage of the destruction of the layer, i.e. the percentage of the layer that is destroyed in relation to the complete layer. Twelve samples are not affected by the reactivation of the catalyst and six samples are.

During the reactivation process with the hydrochloric acid, a total of 17% (2·1+2·2+5+6) of the layer of all eighteen samples is removed. The percentages are not relative to the destruction of the hydrolytic reaction, but the absolute destruction, compared to the untouched layer. Both destruction steps leave the same amount of samples untouched (figure 4.22). Meaning that the hydrolytic reaction and the reactivation process both leave twelve out of eighteen samples without any noticeable layer depletion, hence 66,67%.

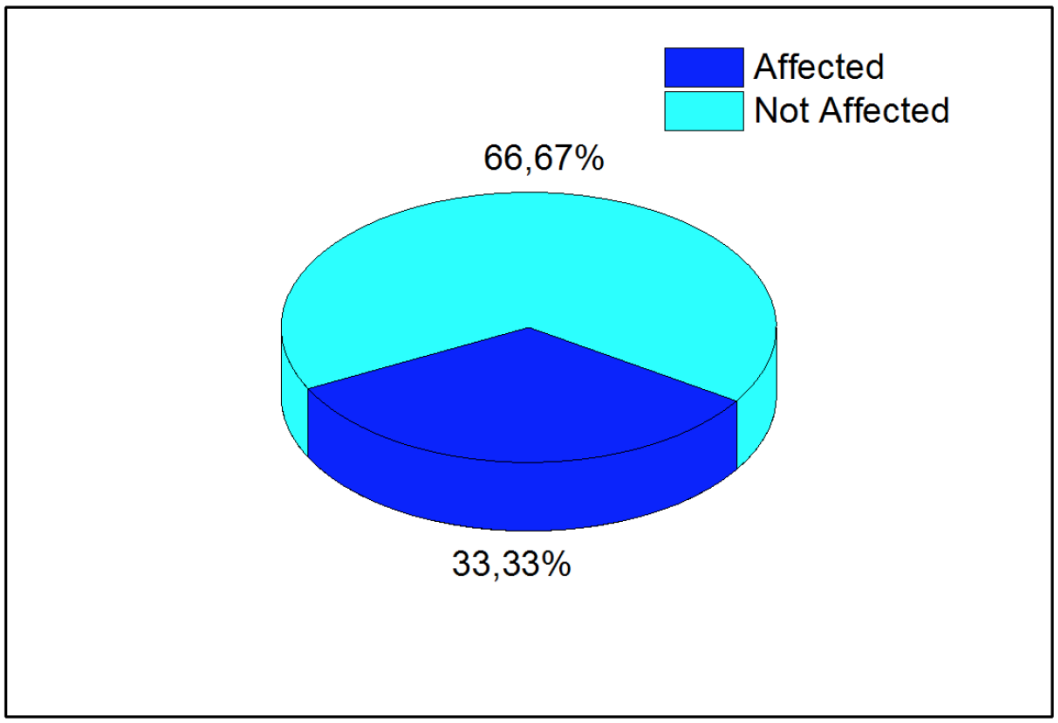

Figure 4.22: Percentage of samples that are affected by the hydrolytic reaction/the reactivation process and percentage of samples that are not affected by the hydrolytic reaction/the reactivation process.

Therefore, a clear statement on the cause of the depletion of the catalyst layer cannot be made. All in all, the samples get six percent more destroyed by the hydrolytic reaction, which is a considerable amount, but both destruction steps destroy six out of eighteen samples. The assumption could be made that the cause of the depletion is the high temperature of the hydrolytic reaction and the hydrochloric-acid water mixture of the reactivation process just washes away the shreds of the catalytic layer that already have been loosened by the hydrolytic reaction.

PML-comp-res-layer

4.3 Theoretical Hydrogen Output of filled HGMS

In this section the theoretical amount of hydrogen that would leave the spheres at different reaction temperatures is discussed. For the hydrogen to leave the spheres a temperature of 250 °C should be applied. This temperature comes from the hydrolytic reaction between sodium borohydride and water in presence of the catalyst TiO_xRu that was sputtered onto the spheres. In the framework of this thesis, the durability of the catalyst during the hydrolytic reaction with empty HGMS was tested. To see how much hydrogen would leave the spheres with the experimentally found temperature curve that reaches a maximum temperature of about 90 °C instead of the suggested 250 °C, the theoretical hydrogen output was calculated.

Hence, the experimentally found temperature curve was used to calculate the amount of hydrogen leaving the HGMS during hydrolysis. The expressions used were the permeability K, the diffusion rate C and pressure p as well as the hydrogen mass n(t) that would leave the spheres.

$$K_i = K_{norm} T_i e^{-Q_k/T_i} \tag{4.1}$$

$$C_i = K_i \frac{3RT_i}{d \cdot r} \tag{4.2}$$

$$B_L = \frac{B_1}{T_L} + \frac{B_2}{T_L^2} \tag{4.3}$$

$$B_E = \frac{B_1}{T_0} + \frac{B_2}{T_0^2} \tag{4.4}$$

$$p_0 = \frac{p_L T_0}{T_L(1 + B_L p_L) - B_E p_L T_0} \tag{4.5}$$

$$p_i = p_{amb} + (p_{i-1} - p_{amb}) e^{-C_i \cdot t_i} \tag{4.6}$$

$$n(t) = \sum_i (p_{i-1} - p_i) \frac{V \cdot M_{H2}}{R \cdot T_i} \tag{4.7}$$

$$1 \leq i \leq 12631$$

Constants			
Permeability K_{norm} [mol/(Pa m s)]	$2{,}787 \cdot 10^{-17}$	Gasconstant R [kg m² /(s² mol K)]	8,314
Activation Energy Q_K [K]	4026	Molarweight of H2 M_{H2} [g/mol]	2,02
Ambient Pressure p_{amb} [Pa]	101325	B_1 (taken from [34])	$2{,}01 \cdot 10^{-6}$
Loading Pressure p_L [Mpa]	85	B_2 (taken from [34])	$-5 \cdot 10^{-7}$
Loading Temperature T_L [K]	523	HMGS Radius r [μm]	1
Extraction Temperature T_0 [K]	300	HMGS Wallthickness d [μm]	0,75
Density of Water ϱ_{H2O} [g/m^3]	10^{-6}	H2 Volume inside 0,8 g HMGS V [μm^3]	1,7
HMGS Mass for one reaction m_{HGMS} [g]	0,8	Gravimetric Storage Capacity γ_G [%]	8,457

Table 4.2: Used constants.

Inserting the parameters from table 4.2, the time t_1=0,25 s and a temperature $T_1 = 300$ K into the expressions 4.1 - 4.7 above, leads to a permeability K_1 of $1{,}25 \cdot 10^{-20}$ mol/(Pa m s), a diffusion rate of $1{,}25 \cdot 10^{-5}$ 1/ s, a loading coefficient B_L of $3{,}84 \cdot 10^{-9}$, an extraction coefficient B_E of $6{,}69 \cdot 10^{-9}$ and an extraction pressure p_1 of 48 MPa. The experiment of the hydrolytic experiment lasted 3600 s, which leads to 12631 data points. The complete mass of hydrogen that would theoretically leave the spheres at the hydrolytic reaction is n(t) and amounts to 0,002 g, if the temperature curve T_i is displayed in figure 4.23 is used, hence the temperature curve of sample 02. The maximum mass of hydrogen that can be loaded into the spheres

is 0,068 g, which can be calculated with following equation.

$$m_{max} = m_{HGMS} \cdot \gamma_G \tag{4.8}$$

If 0,002 g of hydrogen would leave the spheres, this would mean that only 3% of the hydrogen that could be loaded into the spheres would leave the spheres. In the set-up of the experiment the hydrogen is not measured explicitly, but implicitly over the pressure it executes on water. The weight of the water is then measured on a balance (section 3). Hence, a hydrogen mass n(t) of 0,002 g would be a water mass m_{H2O} of 21 g on the balance. This can be calculated with the ideal gas equation.

$$m_{H2O} = \frac{n(t)RT_0}{M_{H2}p_{amb}\varrho_{H2O}} \tag{4.9}$$

The weight of the water varies approximately ± 20 g at each hydrolysis experiment taken. Therefore, 21 g would not be sufficient to discriminate between the hydrogen coming from the hydrolytic reaction and the one leaving the spheres. One can conclude that the hydrogen that would leave the loaded spheres is not traceable with the temperature curves measured in the hydrolysis experiments so far. It is fair to make the assumption that the other 97 % of the hydrogen initially loaded into the HGMS are still in the spheres. It is assumed that a minimum of 10% of the theoretical initial load has to leave the spheres to be able to clearly detect the amount of hydrogen that would come from the spheres. Simulations show that more hydrogen would leave the spheres when the width of the temperature peak is larger, i.e. when the peak reaction temperature is maintained in the three-necked-round-bottom-flask longer. A step-function, as visible in figure 4.23, was used to approximate a temperature curve with a wider peak. For the step-function the assumption was made that the ambient temperature is 25 °C and the extraction temperature of 93 °C is lasting

for 4,2 min. This step-function leads to the same pressure as the real temperature curve, as visible in figure 4.26.

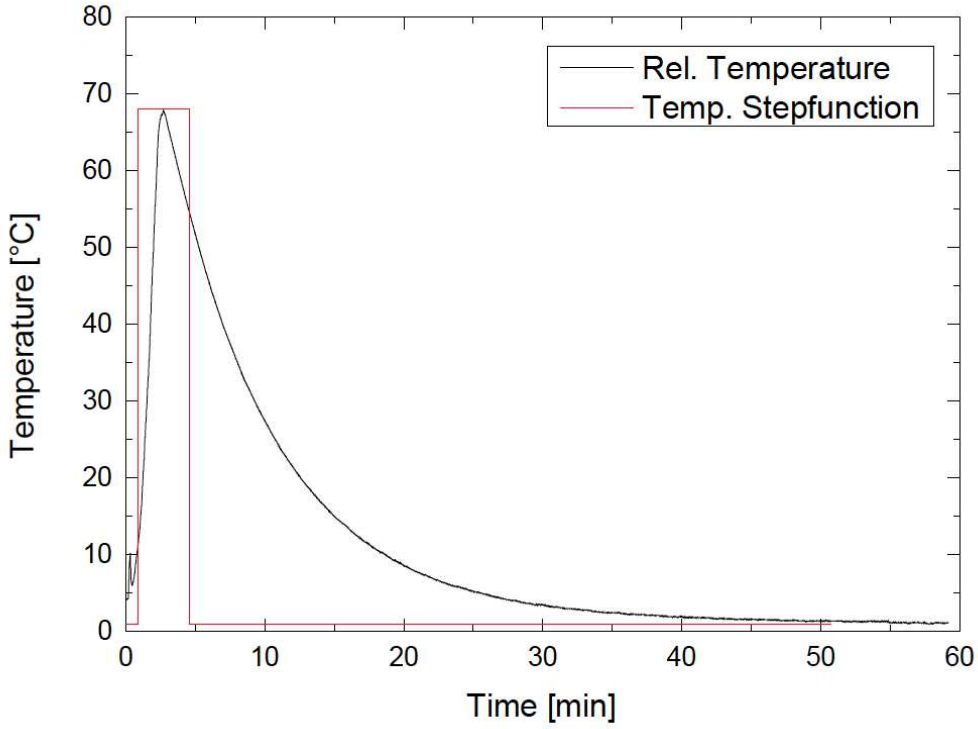

Figure 4.23: Temperature curve from the hydrolytic reaction and the step-function that aims to simulate the temperature curve.

To see how long the maximum relative temperature of 68 °C would have to be maintained inside the spheres, to extract 10% of the hypothetical initial hydrogen load of the spheres, four different pressure curves were simulated with the step-function 4.23. The width of the step-function plateau, i.e. the time the maximum temperature stays in the reaction chamber was varied. For the external heating that was also considered, instead of the width, the height of the step-function plateau was varied. The pressure within the reaction chamber for two different step-functions with temperature peak widths of 60 min (constant temperature of 68 °C) and 16,6

min, as well as a hypothetical external heating of 28 °C were compared to the pressure for the step-function of the uninsulated flask with a temperature peak width of 4,2 min and was plotted against time (figure 4.24). The external heating and the peak temperature step-function peak width of 16,6 min both lead to a hydrogen yield of about 10%.

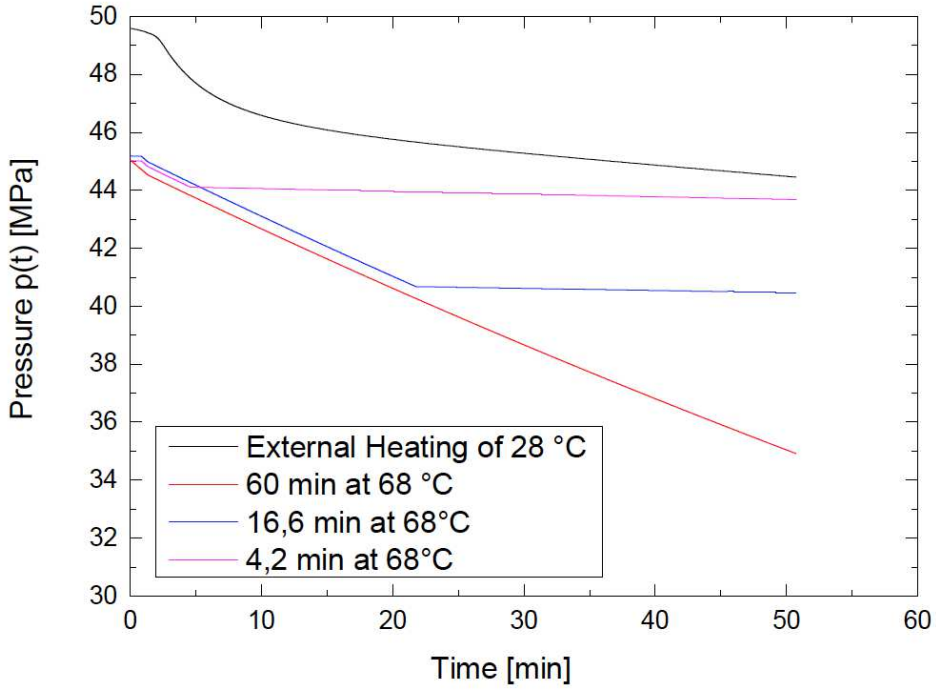

Figure 4.24: Pressure plotted against time for a hypothetical external heating of 28 °C and three different peak widths (60 min, 16,6 min and 4,2 min).

The calculated pressure was used to calculate the respective amounts of hydrogen released (table 4.3). Table 4.3 shows that at a constant temperature of 68 °C throughout the 60 min long experiment, 23 % of the hydrogen that could be loaded into the spheres would leave the spheres. With a temperature peak width of 16,6 min or with an external heating of 28 °C, 10% of the hypothetically loaded hydrogen would leave the spheres. As a comparison, using the uninsulated flask that can be

	Released H_2		
	[g]	[%]	[g] H_2O
Ext. Heating	0,006	10	74
60 min at 68 °C	0,01	23	143
16,6 min at 68 °C	0,006	10	67
4,2 min at 68 °C	0,002	3	19

Table 4.3: Amount of hydrogen leaving the spheres with different temperature curves. [g] H2O refers to the circumstance that the set-up of the hydrolysis experiment is of such that the amount of hydrogen released during hydrolysis is measured by the pressure the hydrogen applies on the water. Thus, experimentally the amount of hydrogen is measured by the weight of the water on the balance (see section 3.2).

simulated with a step-function with a peak width of 4,2 min, 3% of its theoretical initial load would be released. Hence, to get 10% of the theoretical initial load out of the spheres, either an external heating of 28 °C has to be applied, or a temperature of 68 °C needs to stay inside the spheres for 16,6 min.

To put the theoretical results into practice, experiments with an insulated three-necked-round-bottom-flask (where the reaction takes place) were made. To keep the heat inside the flask, a Styrofoam isolation was used, as shown in figure 3.3. Figure 4.25 shows a comparison between the temperature curves of the reaction in an insulated and uninsulated three-necked-round-bottom-flask, plotted against time. The peak temperature of the reaction inside the insulated flask is 3 °C higher than the temperature inside the uninsulated flask. Furthermore, the peak width is significantly larger. Figure 4.26 shows the pressure curves of the insulated and uninsulated flask, as well as the pressure curves for the 4,2 min and 7,1 min step-function, plotted against time. The pressure curve for the uninsulated flask is in good accordance with the pressure curve for the 4,2 min step-function and the curve for the insulated flask correlates with the curve for the 7,1 min step-function.

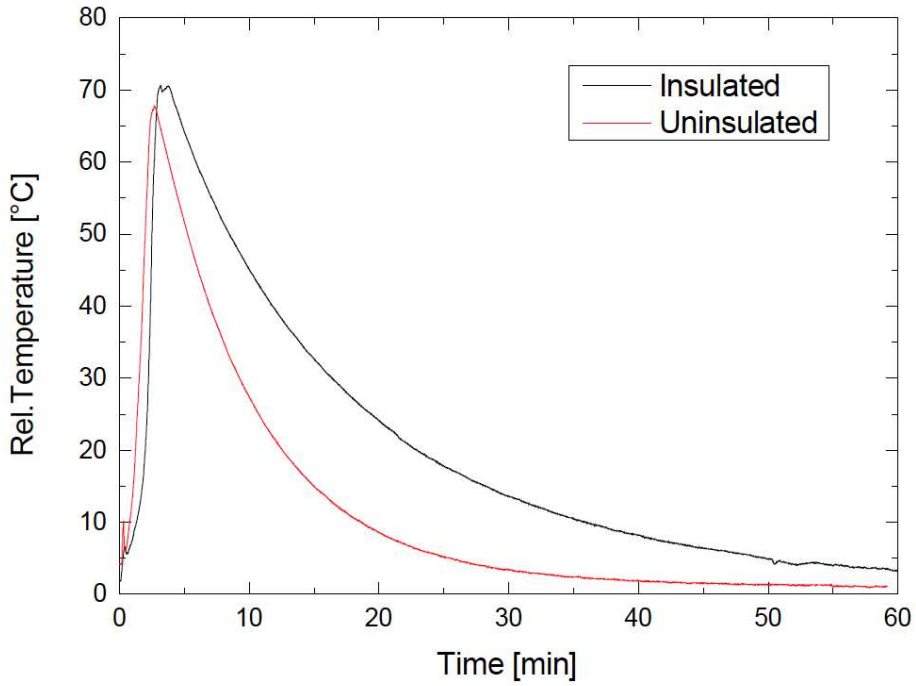

Figure 4.25: Temperature curves measured in an insulated and uninsulated three-necked-round-bottom-flask.

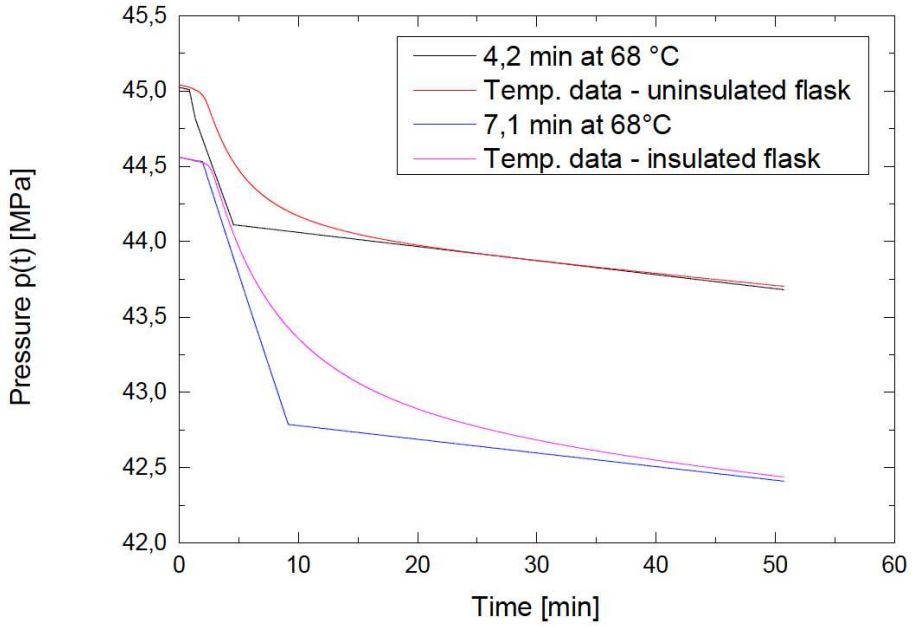

Figure 4.26: Pressures plotted against time for temperature curves measured in an uninsulated and insulated three-necked-round-bottom-flask and comparison with the theoretical pressure curves using the step-function temperature curve (figure 4.23).

	Released H_2		
	[%]	[g]	[g] H_2O
4,2 min	3	0,002	20
uninsulated	3	0,002	20
7,1 min	5	0,003	36
insulated	5	0,003	36

Table 4.4: Amount of hydrogen leaving the spheres with different temperature curves (temperature curves using the insulated and uninsulated reaction chamber as well step-function temperature curves with a 4,2 min and 7,3 min peak width)

The calculations of the amount of hydrogen leaving the spheres is displayed in table 4.4 for all four pressure curves. The calculations show that the step-function is a good approximation of the experimental temperature curve. The insulated flask

enables the HGMS to release 5% instead of 3% of its initially loaded hydrogen, which corresponds to a weight of 0,003 g H_2, leading to 36 g H_2O on the balance. An amount of 36 g could be significant enough to stand out against the deviations of about ± 20 g of the weight of the water on the balance that indicates the weight of the hydrogen leaving the spheres. Hence, the hydrogen leaving the spheres inside an insulated flask could be significant enough to be traced.

5 Conclusion

Within the hybrid hydrogen storage solution described in this thesis, the catalyst is sputter coated onto the HGMS. For efficiency and economical reasons, the HGMS are to be used as many times as possible. So far, the hydrolysis is found to be working four times with the same HGMS (figure 4.4). It is assumed that the hydrolysis stops working after the fourth hydrolytic reaction because the catalyst wears off (figure 2.2). Experiments on the destructibility of the catalyst layer show that humidity has no influence on the catalyst layer. It is the hydrolytic reaction between $NaBH_4$ and water and the hydrochloric acid - water bath that wears the catalyst layer off. It cannot be clearly determined which of the two steps of the hydrolytic cycle is damaging the catalyst layer more. It seems like the two processes are depleting the catalyst layer equally. However, it can be assumed that the high temperatures of the hydrolytic reaction cracks the surface of the catalyst layer and the hydrochloric-acid water mixture rinses off the last shreds of the thin-film. Destruction experiments with varying bonding agent thicknesses show that the bonding agent needs to be of a minimum thickness of 0,5 nm. Thicknesses above 0,5 nm do not show a significant increase of performance (figures 4.19 and 4.11). Calculations on the hydrogen yield from the hollow micro glass spheres show that the hydrogen yield is bigger when the reaction chamber is insulated. In other words, when the heat of the hydrolytic reaction stays in the reaction chamber longer, more hydrogen leaves the spheres. The amount of hydrogen leaving the spheres increases from 3% to 5% of the initial

amount of hydrogen loaded into the spheres and from 20 g of water on the balance to 36 g. The hydrogen coming from the hydrolytic reaction has a variation of ±20 g at each hydrolytic reaction. Therefore, 20 g and possibly also 36 g is a non-measurable amount of hydrogen, as it could not be differentiated from the fluctuations of the hydrogen that is produced by the hydrolytic reaction. A measurable amount of hydrogen leaving the spheres was considered to be 10% of the theoretical initial load. To get 10% of the hydrogen that could be loaded into the spheres out of the spheres, an external heating of 28 °C has to be applied, or a temperature of 68 °C needs to stay inside the spheres for 16,6 min. Finding a better isolation for the reaction chamber or applying an external heat of 28 °C to further increase the temperature in the reaction chamber, could be a matter of future research.

List of Figures

List of Tables

Bibliography

[1] William Ruddiman. Plows, Plagues, and Petroleum: How Humans Took Control of Climate. Princeton University Press, 2016.

[2] David Lochbaum, Edwin Lyman, and Susan Stranahan. Fukushima: The Story of a Nuclear Disaster. The New Press, 2014.

[3] David Pimentel, Alison Marklein, Megan Toth, and Tim Krueger. Food versus biofuels: Environmental and economic costs. Human Ecology, 37:1, 2009.

[4] Marcelo Carmo, David L. Fritz, Jürgen Mergel, and Detlef Stolten. A comprehensive review on pem water electrolysis. International Journal of Hydrogen Energy, 38(12):4901–4934, 2013.

[5] Solar hydrogen cycle house demo. https://www.fuelcellstore.com/h-tec-demo-house-d111. Accessed: 12/2018.

[6] Susanne Planitzer-Rehm. Prüfung der katalysatorschichthaftung auf hohlen mikroglaskugeln bei katalytischer hydrolyse mit nabh4, 2018. Bachelorthesis.

[7] Gerwin Schmid. A hybrid hydrolytic hydrogen storage system based on catalyst sputtercoated hollow glass microspheres. PhD thesis, 2015.

[8] I. Sreedhar, Krutarth M. Kamani, Bansi M. Kamani, Benjaram M. Reddy, and A. Venugopal. A birds eye view on process and engineering aspects of hydrogen storage. Renewable and Sustainable Energy Reviews, 91:838–860, 2018.

[9] Jose Bellosta Von Colbe, Jose-Ramón Ares, Jussara Barale, Marcello Baricco, Craig Buckley, Giovanni Capurso, Noris Gallandat, David M. Grant, Matylda N. Guzik, Isaac Jacob, and et al. Application of hydrides in hydrogen storage and compression: Achievements, outlook and perspectives. International Journal of Hydrogen Energy, 2019.

[10] Lei Wang, Aditya Rawal, and Kondo-Francois Aguey-Zinsou. Hydrogen storage properties of nanoconfined aluminium hydride (alh3). Chemical Engineering Science, 194:64–70, 2019.

[11] Alireza Rahnama, Guilherme Zepon, and Seetharaman Sridhar. Machine learning based prediction of metal hydrides for hydrogen storage, part i: Prediction of hydrogen weight percent. International Journal of Hydrogen Energy, 44(14):7337–7344, 2019.

[12] Jiguang Zhang, Yunfeng Zhu, Linglong Yao, Cheng Xu, Yana Liu, and Liquan Li. State of the art multi-strategy improvement of mg-based hydrides for hydrogen storage. Journal of Alloys and Compounds, 782:796–823, 2019.

[13] Yanping Fan, Dandan Chen, Xianyun Liu, Guangxin Fan, and Baozhong Liu. Improving the hydrogen storage performance of lithium borohydride by ti3c2 mxene. International Journal of Hydrogen Energy, 2019.

[14] M.w. Davids, M. Lototskyy, M. Malinowski, D. Van Schalkwyk, A. Parsons, S. Pasupathi, D. Swanepoel, and T. Van Niekerk. Metal hydride hydrogen storage tank for light fuel cell vehicle. International Journal of Hydrogen Energy, 2019.

[15] Qun Luo, Jianding Li, Bo Li, Bin Liu, Huaiyu Shao, and Qian Li. Kinetics in mg-based hydrogen storage materials: Enhancement and mechanism. Journal of Magnesium and Alloys, 2018.

[16] Loris Lombardo, Heena Yang, and Andreas Züttel. Study of borohydride ionic liquids as hydrogen storage materials. Journal of Energy Chemistry, 33:17–21, 2019.

[17] Daniel Teichmann, Wolfgang Arlt, and Peter Wasserscheid. Liquid organic hydrogen carriers as an efficient vector for the transport and storage of renewable energy. International Journal of Hydrogen Energy, 37(23):18118–18132, 2012.

[18] Deyu Qu, Xiaoduo Xu, Lina Zhou, Wenjing Li, Jorryn Wu, Dan Liu, Zhi-Zhong Xie, Junsheng Li, and Haolin Tang. Electrochemical hydrogen storage in iron nitrogen dual-doped ordered mesoporous carbon. International Journal of Hydrogen Energy, 44(14):7326–7336, 2019.

[19] Ali Salehabadi, Mardiana Idayu Ahmad, Norhashimah Morad, Masoud Salavati-Niasari, and Morteza Enhessari. Electrochemical hydrogen storage properties of ce0.75zr0.25o2 nanopowders synthesized by sol-gel method. Journal of Alloys and Compounds, 2019.

[20] Siemens Magazin. Pooling competencies. Nov 2016. https://www.siemens.com/customer-magazine/en/home/industry/one-step-closer-to-industrie-4-0/new-hydrogen-storage-technology.html.

[21] Hycare focuses on large-scale, solid-state hydrogen storage. Fuel Cells Bulletin, 2019(2):11, 2019.

[22] Miriam Rueda, Luis Miguel Sanz-Moral, and Ángel Martín. Innovative methods to enhance the properties of solid hydrogen storage materials based on hydrides through nanoconfinement: A review. The Journal of Supercritical Fluids, 141:198–217, 2018.

[23] Bo Li, Jianding Li, Huajun Zhao, Xueqing Yu, and Huaiyu Shao. Mg-based

metastable nano alloys for hydrogen storage. International Journal of Hydrogen Energy, 44(12):6007–6018, 2019.

[24] D.p. Broom, C.j. Webb, G.s. Fanourgakis, G.e. Froudakis, P.n. Trikalitis, and M. Hirscher. Concepts for improving hydrogen storage in nanoporous materials. International Journal of Hydrogen Energy, 2019.

[25] Frank J. Isidro-Ortega, Juan H. Pacheco-Sánchez, R. Alejo, Luis A. Desales-Guzmán, and J. Salvador Arellano. Theoretical studies in the stability of vacancies in zeolite templated carbon for hydrogen storage. International Journal of Hydrogen Energy, 44(13):6437–6447, 2019.

[26] Xiongyi Liang, Siu-Pang Ng, Ning Ding, and Chi-Man Lawrence Wu. Strain-induced switch for hydrogen storage in cobalt-decorated nitrogen-doped graphene. Applied Surface Science, 473:174–181, 2019.

[27] Xin Zhang, Shiwei Cao, Ning Zhang, Lei Wang, Ximeng Chen, and Zhan Li. Three-dimensional nanopores on monolayer graphene for hydrogen storage. Materials Chemistry and Physics, 209:134–145, 2018.

[28] Kranthi Kumar Gangu, Suresh Maddila, Saratchandra Babu Mukkamala, and Sreekantha B Jonnalagadda. Characteristics of mof, mwcnt and graphene containing materials for hydrogen storage: A review. Journal of Energy Chemistry, 30:132–144, 2019.

[29] S. A. Sherif. Handbook of hydrogen energy. CRC Press, 2015.

[30] R Teitel. Hydrogen supply method, Jul 1980.

[31] Xiaobo Qi, Cong Gao, Zhanwen Zhang, Sufen Chen, Bo Li, and Sheng Wei. Production and characterization of hollow glass microspheres with high dif-

fusivity for hydrogen storage. International Journal of Hydrogen Energy, 37(2):1518–1530, 2012.

[32] 3M Energy and Advanced Material Division. http://multimedia.3m.com/mws/media/694361O/3m-glass-bubbles-s38.pdf, May 2017. Accessed: 01/2019.

[33] Masayuki Nogami, Junji Hayakawa, and Yoshiro Moriya. Fabrication of hollow glass microspheres in the na2o-b2o3-sio2 system from metal alkoxides. Journal of Materials Science, 17(10):2845–2849, 1982.

[34] Honggang Chen, Jinyang Zheng, Ping Xu, Lei Li, Yanlei Liu, and Haiyan Bie. Study on real-gas equations of high pressure hydrogen. International Journal of Hydrogen Energy, 35(7):3100–3104, 2010.

[35] M Keding and M Tajmar. Method and installation for storing and releasing hydrogen, Feb 2008.

[36] David R. Lide. CRC handbook of chemistry and physics: a ready-reference book of chemical and phyical data. CRC Press, 1992.

[37] Yoshitsugu Kojima, Ken-Ichirou Suzuki, Kazuhiro Fukumoto, Megumi Sasaki, Toshio Yamamoto, Yasuaki Kawai, and Hiroaki Hayashi. Hydrogen generation using sodium borohydride solution and metal catalyst coated on metal oxide. International Journal of Hydrogen Energy, 27(10):1029–1034, 2002.

[38] Katalysator. http://www.chemie.de/lexikon/Katalysator.html. Accessed: 03/2019.

[39] Hari Singh Nalwa. Handbook of thin film materials. Deposition and processing of thin films. Academic Press, 2001.

[40] Diederik Depla and Stijn Mahieu. Reactive Sputtering Deposition. Springer, 2008.

[41] Digital microscope ge-5. url=https://www.sios.net.au/microscope-camera-systems/small-digital/digital-microscope-ge-5. Accessed: 05/2019.

[42] Polyvar met light microscope. url=http://www.materials.co.uk/optical.htm. Accessed: 05/2019.